STRUCTURAL ANALYSIS OF PROGRESSIVE DEFORMATION WITHIN A COMPLEX STRIKE-SLIP FAULT SYSTEM: SOUTHERN NARRAGANSETT BASIN, RHODE ISLAND

APPROVED:

Sharon Bosher

W R Muehlberger

William D. Carlson

# STRUCTURAL ANALYSIS OF PROGRESSIVE DEFORMATION WITHIN A COMPLEX STRIKE-SLIP FAULT SYSTEM: SOUTHERN NARRAGANSETT BASIN, RHODE ISLAND

BY

ALAN WALTER BERRYHILL, B.S.

THESIS

Presented to the Faculty of the Graduate School of

The University of Texas at Austin

in Partial Fulfillment

of the Requirements

for the Degree of

MASTER OF ARTS

THE UNIVERSITY OF TEXAS AT AUSTIN

MAY, 1984

ACKNOWLEDGMENTS

I would like to thank Dr. Sharon Mosher, who supervised this work, for her countless hours of help, advise, and encouragement. Helpful consultations with Professors William D. Muehlberger, William Carlson and Mark Cloos, are also acknowledged. Ed Cazier served as student editor.

Funding for the field portion of this study was provided through a National Science Foundation Grant for the Narragansett Basin Project (1982). Lodging while in the field was provided by the Ft. Getty Recreation Area and the town of Jamestown, Rhode Island.

Finally, I would like to thank my parents for their continual support throughout my academic career. This study would not have been possible without the help, friendship and fishing wizardry of Rachel Burks (Burks and Shaler, in prep.).

ABSTRACT

Complex progressive ductile deformation on Dutch Island, Narragansett Basin, Rhode Island, is localized along a system of non-parallel strike-slip faults with opposite senses of motion. The structural intensity and complexity of this area can be attributed in part to the proximity of NE- and NNE-trending, preexisting basement faults bounding early horsts and grabens. Left-lateral faults in NNE to NE orientations correspond to R′ riedel shears and right lateral faults in NE to ENE orientations correspond to right-lateral primary shears within an E-trending right-lateral transform system. Structural superposition of mesoscopic folds and incremental crenulation cleavages, formed due to episodic movement along these faults, indicates that left-lateral motion preceded right-lateral motion and that many NE-trending faults underwent first left-lateral and then right-lateral movement.

As many as 8 sets of discrete superposed crenulation cleavages and 7 sets of discrete mesoscopic folds were developed at fault intersections on the island. Preservation of these structures can be attributed to the presence of a strong preexisting structural and metamorphic fabric which formed as a result of initial basin closure associated with the collision of the African and North American continents in the late Paleozoic. Study of geometry and overprinting relations of the fold and crenulation sets within adjacent shear zones served to track movement along individual faults through time. Up to 32 degrees of anticlockwise internal rotation on left lateral faults and clockwise rotation on right-lateral faults has occurred. Discrete crenulations form due to flexural slip at an angle to

the shear plane and are subsequently tightened and rotated toward the principal extensional strain direction untl flexural slip can no longer occur. A younger set then forms and overprints the preexisting, and presently locked, crenulation cleavage at an angle varying from 4 to 22 degrees.

Structural analysis of the complex deformation on Dutch Island indicates that accurate tracking of fault motion within complex shear systems is feasible in areas in which overprinting relations between progressive deformations are preserved. In addition to the regional significance of the study, the structural styles and deformation patterns described on Dutch Island should be analagous to what might be expected in a larger block caught within a system of non-parallel, successively forming strike-slip faults.

TABLE OF CONTENTS

# LIST OF FIGURES

## LIST OF TABLES

# INTRODUCTION

The Narragansett Basin of Rhode Island and Massachussetts (Fig. 1) is a critical area for the understanding of the Alleghanian Orogeny in the northern Appalachians. Many workers (Mosher and Wood, 1976; Skehan and Murray, 1979; McMaster and others, 1980; Burks, 1981; Burks and others,1981; Mosher, 1981, 1983a; Farrens, 1982; Thomas, 1982) have studied the structure within the Narragansett Basin in an attempt to determine the precise tectonic history and setting of New England in the late Paleozoic. In the northern part of the basin, the rocks are mildly deformed, whereas in the southern basin, the rocks have undergone a complex sequence of deformations. Much of this deformation is apparently related to strike-slip faulting, which localizes intense deformation along major shear zones (Mosher, 1983b). Clearly, a record of relative movement along these faults through time would contribute to and refine tectonic models for deformation of the Narragansett Basin, and would explain many of the complex structures found in the southern basin. The detailed structural study reported here was conducted adjacent to one of these complex shear systems in order to determine the deformational sequence of events of both folding and faulting, and to relate both the structures and their relative times of occurrence to the tectonic framework for the Narragansett Basin in the late Paleozoic.

This study examines Dutch Island, located in southwestern Narragansett Basin, within the Beaverhead Shear Zone (Fig. 1). The island is a fault-bounded horst block, eroded to its present state by Pleistocene glaciation. The rocks on Dutch Island preserve a deformational sequence as

intense and complex as is found anywhere in the basin. Two distinct generations of strike-slip faults with opposite senses of motion generated two major progressive deformations, overprinting a preexisting metamorphic and structural fabric. This study combines a geometric analysis of microscopic and mesoscopic structures found on Dutch Island with a comparative study of incremental strains produced during progressive deformation within a shear zone to determine the precise movement history of strike-slip faulting events in the southern Narragansett Basin. The structural descriptions and interpretations are presented topically, in chronologic order.

## REGIONAL GEOLOGY AND TECTONIC SETTING

The Narragansett Basin is an elongate structural basin believed to be part of a NE-trending chain of pull-apart grabens extending offshore to the NE and SW under Long Island Sound (McMasters and others, 1980; Mosher, 1983b). The basin may have formed as a result of interaction between the Avalonian microcontinent and North America along a NNE-trending, left-lateral shear system (McMasters and others, 1980; Mosher, 1983b) and lies at the juncture of two late Paleozoic foldbelts, the Variscan and the Caledonian, which merge to form the Appalachians in North America. Up to 3700 meters of Pennsylvanian non-marine sediments fill the basin (Mutch, 1968), deposited syntectonically as the basin opened as a composite graben (Mosher, 1983b).

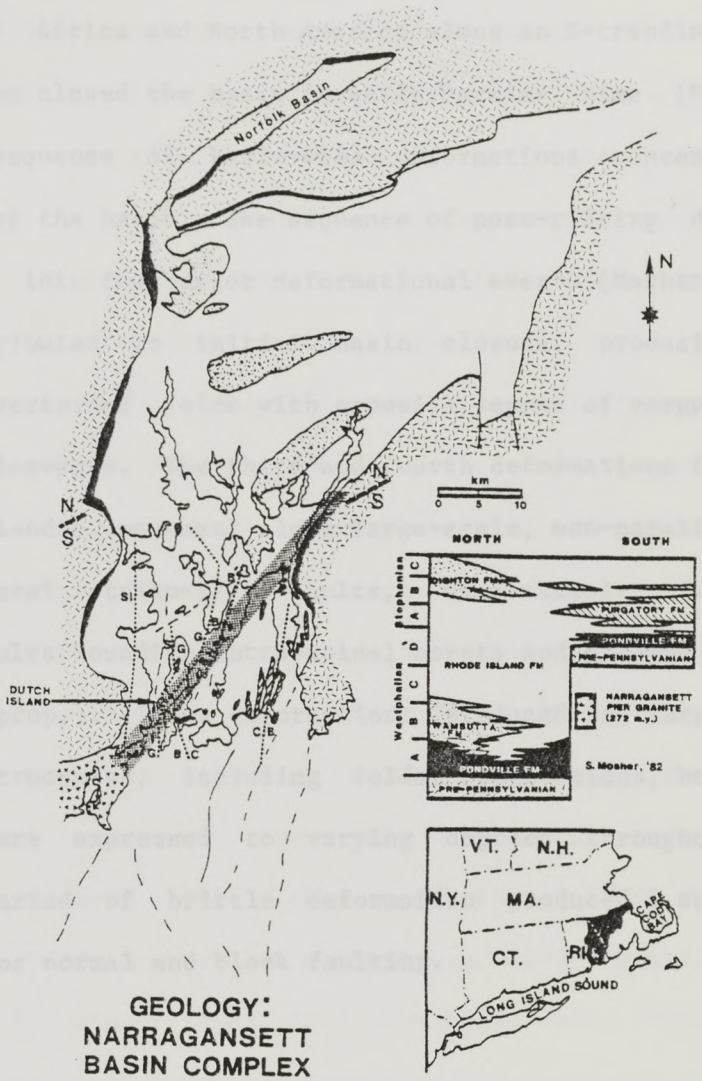


Fig. 1. Geologic map of the Narragansett Basin complex showing distribution of lithologies, metamorphic isograds, and basin location. Beaverhead shear zone (BHSZ) is stipled; boundaries of metamorphic isograds (C, chlorite; B, biotite; G, garnet; S, staurolite; Si, sillimanite) are dotted. Approximate location of northern and southern graben boundary is indicated with N/S. Stratigraphic column shows relative time stratigraphic units. After Mosher (1983).

Following initial rifting and subsequent filling of the basin, convergence of Africa and North America along an E-trending right-lateral transform system closed the basin in early Permian time (Mosher, 1983a), producing a sequence of basin-wide deformations concentrated in the southern part of the basin. The sequence of post-rifting deformation may be subdivided into four major deformational events (Mosher, 1983): D1 and D2 may be attributed to initial basin closure, producing large-scale upright to overturned folds with opposite senses of vergence, and strong axial planar cleavages. The third and fourth deformations (D3 and D4) were caused by episodic movement along large-scale, non-parallel left-lateral and right-lateral strike-slip faults, respectively, which may be reactivated faults bounding intrabasinal horsts and grabens (Mosher, 1983b; Henderson, in prep.). These deformations produced a large and complex variety of structures, including folds, crenulations, boudins, and kink bands, which are expressed to varying degrees throughout the basin. Finally, a period of brittle deformation produced 2 sets of conjugate joints and minor normal and block faulting.

## PREVIOUS WORK

Prior to this study, only reconnaissance lithologic and structural mapping had been conducted on Dutch Island. Shaler and others (1899) listed and described the basic lithologies on Dutch Island, and assigned a Pennsylvanian age to the metasediments, based on plant fossil identification. Preliminary structural mapping by Burks (1981) and Murray

(1982) indicated a highly complex structural history, possibly similar to the deformational sequence found on nearby Beaverhead (Skehan and Murray, 1979; Burks, 1981, 1981a; Berryhill, 1983, in press). Skehan and Murray (1979) attribute areas of intense deformation in the southern basin to close proximity to major strike-slip faults, and Mosher (1983) proposed a kinematic model for the Narragansett Basin which allows for the structural intensity and complexity found on Dutch Island.

This study applies strain modelling and deformation analysis techniques to a complex ductile shear system on and surrounding Dutch Island, Rhode Island. In this regard, a number of structural studies in other areas were helpful in understanding the structure of Dutch Island, particularly those modelling strain paths and deformation geometries in complex shear zones (Ramsay, 1967; Coward, 1976; Ramsay and Graham, 1970; Ramsay, 1980; Skjernaa, 1980). In addition, other studies dealing with reorientation of structures and fold rotation during progressive deformation (Sanderson, 1973; Wilcox and others, 1973; Rhodes and Gayer, 1977; Williams, 1978; Ramsay, 1979; Sanderson, 1979; Helmstaedt and Dixon, 1980; Bell, 1981; Winsor, 1979, 1981; Beach and Jack, 1982; Hanmer, 1981), as well as theoretical studies of incremental deformation mechanics (Biot, 1965) were helpful. Another relevant experimental study used is that by Ramberg (1964) which showed that simultaneous formation of multiple orders of folds can occur due to rheological variations. The field area of the present study is unique in that an extremely complex deformational sequence has been preserved which allows detailed tracking of strike-slip fault movement through time and which also reflects a regional tectonic framework.

## FIELD TECHNIQUES

Dutch Island has continous outcrop along three-quarters of the island's margin (Fig. 2), allowing detailed structural mapping at a scale varying from 1:60 to 1:1200, depending on outcrop quality and structural complexity. The majority of the island's interior is covered by glacial till and dense vegetation, so structural trends there were inferred from marginal outcrop and bedrock topography. The scale of mapping conducted on Dutch Island allowed discrimination of small scale structures which might have been lumped together in a more regional study. In addition, joint surfaces produced three-dimensional exposures around much of the island, so that precise measurements of fold axes and cleavage planes were possible. This three-dimensional geometric analysis aided considerably in differentiating similar structures produced during progressive deformation.

## LITHOLOGY

The rocks exposed on Dutch Island (Fig. 2) lie within the Pennsylvanian Rhode Island Formation (Mutch, 1968; Fig. 1). All rocks on Dutch Island exhibit metamorphic mineral assemblages within the almandine zone and have undergone varying degrees of retrograde metamorphism and chloritization. The major lithologies on Dutch Island may be summarized as follows:

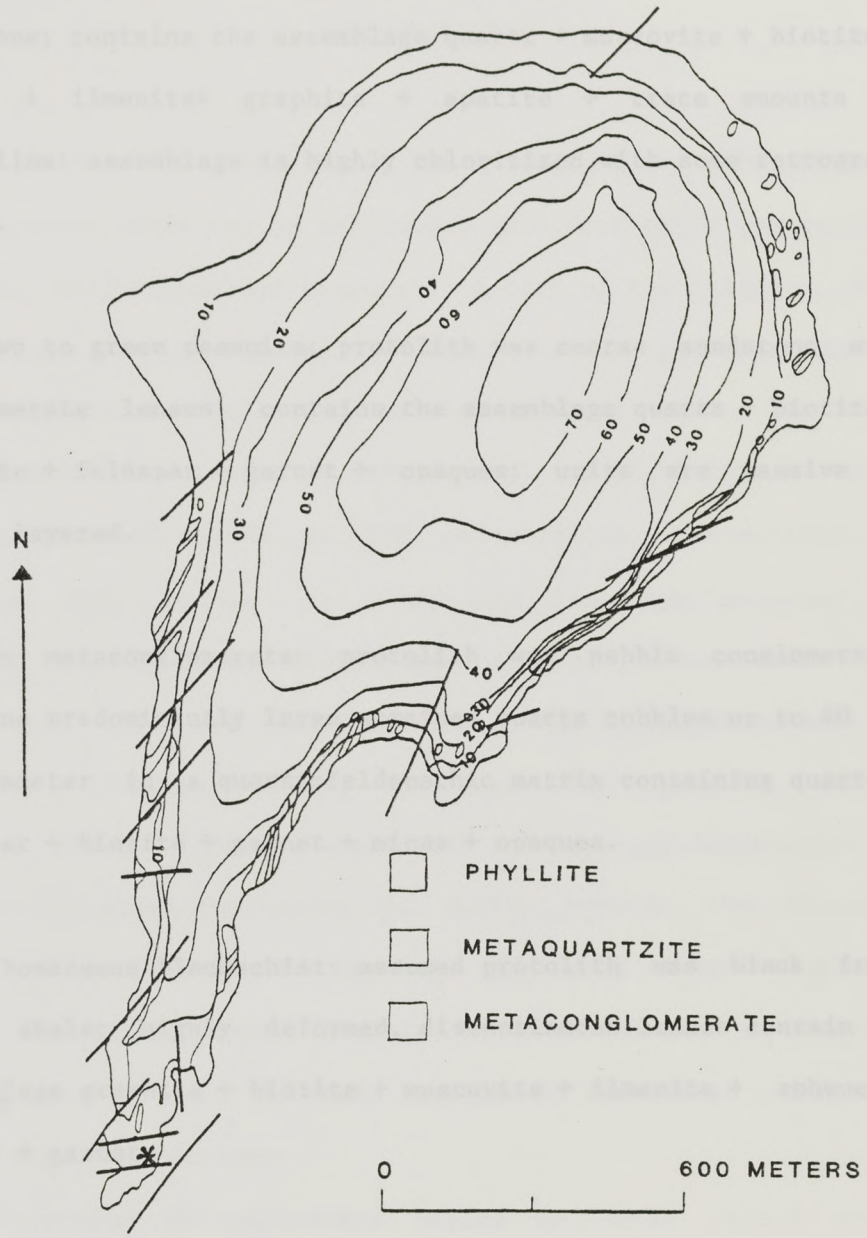


Fig. 2. Lithologic map of Dutch Island. Major lithologies are shown in the key. Lenses of graphite and calc-silicates are also present, but are discontinuous and less than 1 meter thick. Countour interval for this and other figures is 10 feet. Location of samples DI-5a and DI-12 (see Appendix I) are indicated by (*).

1. Gray to black phyllite: protolith was silty shale to siltstone; contains the assemblage quartz + muscovite + biotite + garnet + ilmenite+ graphite + apatite + trace amounts of tourmaline: assemblage is highly chloritized with some retrograde sphene.

2. Brown to green psammite: protolith was coarse sandstone with conglomerate lenses; contains the assemblage quartz + biotite + chlorite + feldspar + garnet + opaques; units are massive to finely layered.

3. Tan metaconglomerate: protolith was pebble conglomerate; contains predominantly large strained quartz cobbles up to 40 cm in diameter in a quartzofeldspathic matrix containing quartz + feldspar + biotite + garnet + micas + opaques.

4. Carbonaceous blackschist: assumed protolith was black fresh water shale; highly deformed, discontinuous lenses contain the assemblage graphite + biotite + muscovite + ilmenite + sphene + quartz + garnet.

5. Green calcsilicate pods: protolith was fresh water carbonates; found in discontinuous pods interbedded with psammite or phyllite units; contains the assemblage quartz + hornblende + feldspar + diopside + opaques.

# STRUCTURE

## INTRODUCTION

The deformational history of Dutch Island after the formation of the Narragansett Basin may be subdivided into four major events, resulting in a complex, well-documented kinematic history of the island. The first two events may be attributed to basin closure, producing two or three generations of discrete folds and associated structures. The third and fourth deformations were due to left-lateral and right-lateral strike-slip faulting in NNE to NE and NE to ENE orientations, respectively. These deformations fit within the tectonic framework proposed for the Narragansett Basin by Mosher (1983b) and similar deformational sequences were described elsewhere in the basin in field studies by Burks (1981), Thomas (1981), Farrens (1982), Henderson (in prep.), and Mosher (unpublished work). Thus, the sequence and style of deformation found on Dutch Island is not unique within the basin; however the intensity and complexity of structures has not been previously recognized elsewhere in the basin. The extraordinary quality of preservation of deformational features allows a detailed field analysis of structures produced under a variety of strain conditions.

An overview of structural styles on Dutch Island shows that deformational complexity and intensity are not uniform across the island. The number and complexity of known and inferred strike-slip faults increases southward (Fig. 3), as does the amount of shear-related deformation, which is generally localized and intensified along fault

planes. Locations of inferred strike slip faults were determined by a combination of outcrop pattern, topographic lineaments, and changes in structural styles, whereas the attitudes of other faults were readily measurable in outcrop. The concentration of shear-related deformation in the southern part of the island (Fig. 4a and 4b) tended to obliterate early deformational features, in which D1 and D2 structures were almost completely transposed. The northern part of the island is somewhat less faulted, and thus less D3 and D4 deformation is present. Early folds (F1 to F4) are found more frequently in the northern part of the island (Fig. 5), and the earliest metamorphic foliation (S1) is more easily differentiated in the north as well. Outcrop in general is better in the southern part of Dutch Island.

The structure of Dutch Island will be described in two major chronologic groups: early deformation and metamorphism, and all deformation related to later strike-slip faulting. A separate section discusses reoriented structures of unknown origin. Early deformation and metamorphism are discussed first because they provide a structural and metamorphic fabric which allowed preservation of the complex shear-related structures.

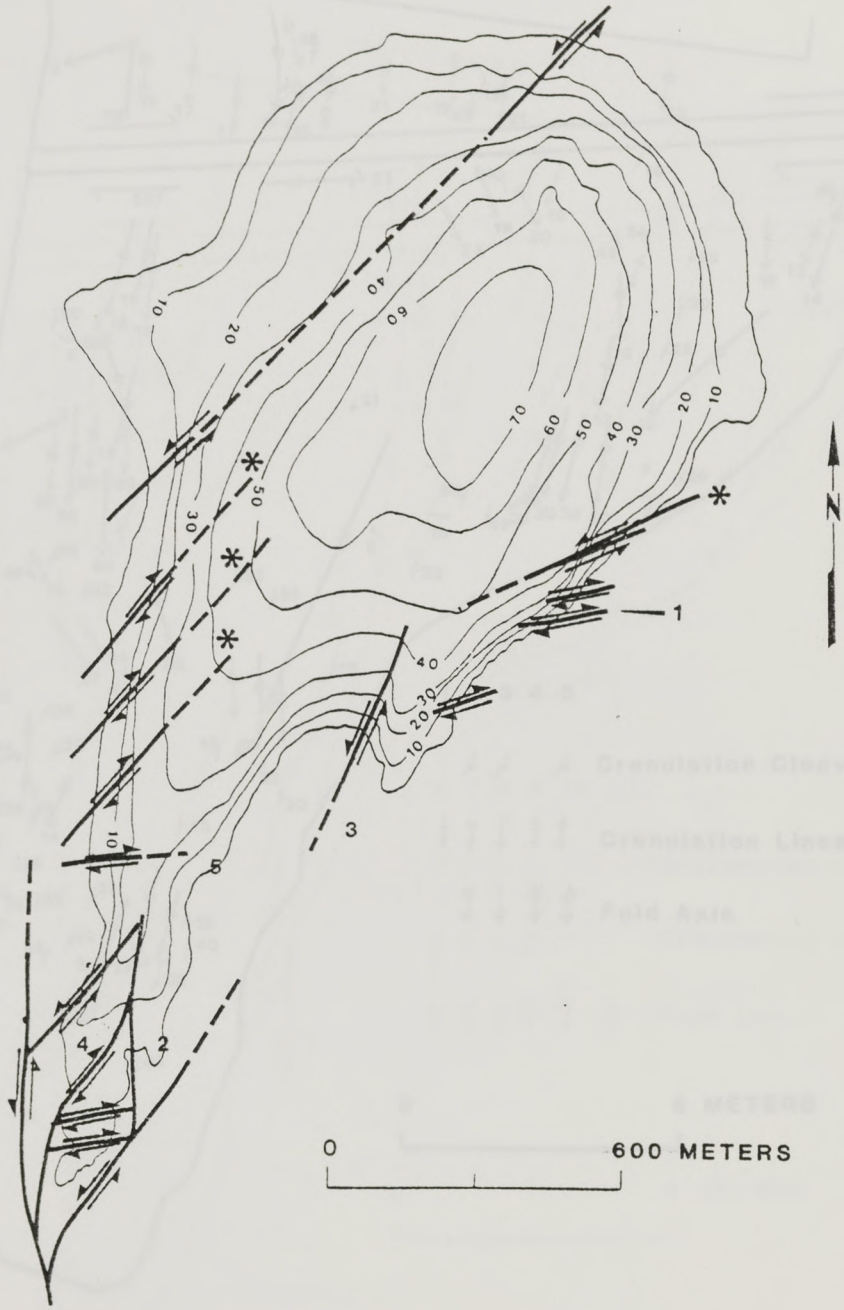


Fig. 3. Strike-slip faults locations and movement directions on Dutch Island. Faults with (*) underwent both left-lateral and right-lateral motion. Only the first episode of movement is indicated. Numbered faults are described in detail in the text. The location of the detailed maps in Fig. 4a and 4b are shown.

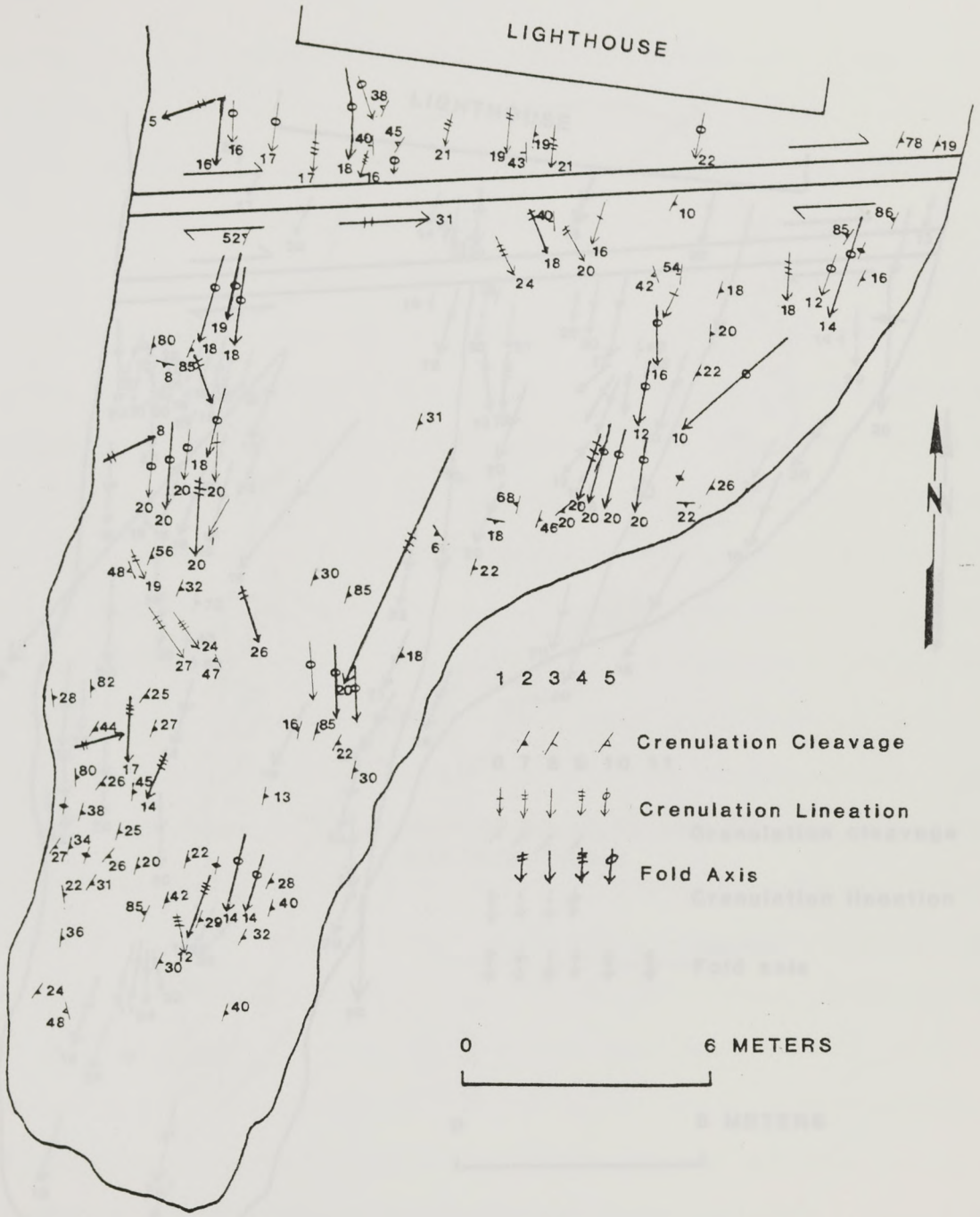


Fig. 4a. Detailed structural map of southernmost Dutch Island. The most complex structure on the island is preserved here, and mapping was conducted at a scale of 1:60. Mesoscopic folds are shown in thicker lines. Fold and crenulation numbers indicated in the explanation correspond to deformation descriptions in text.

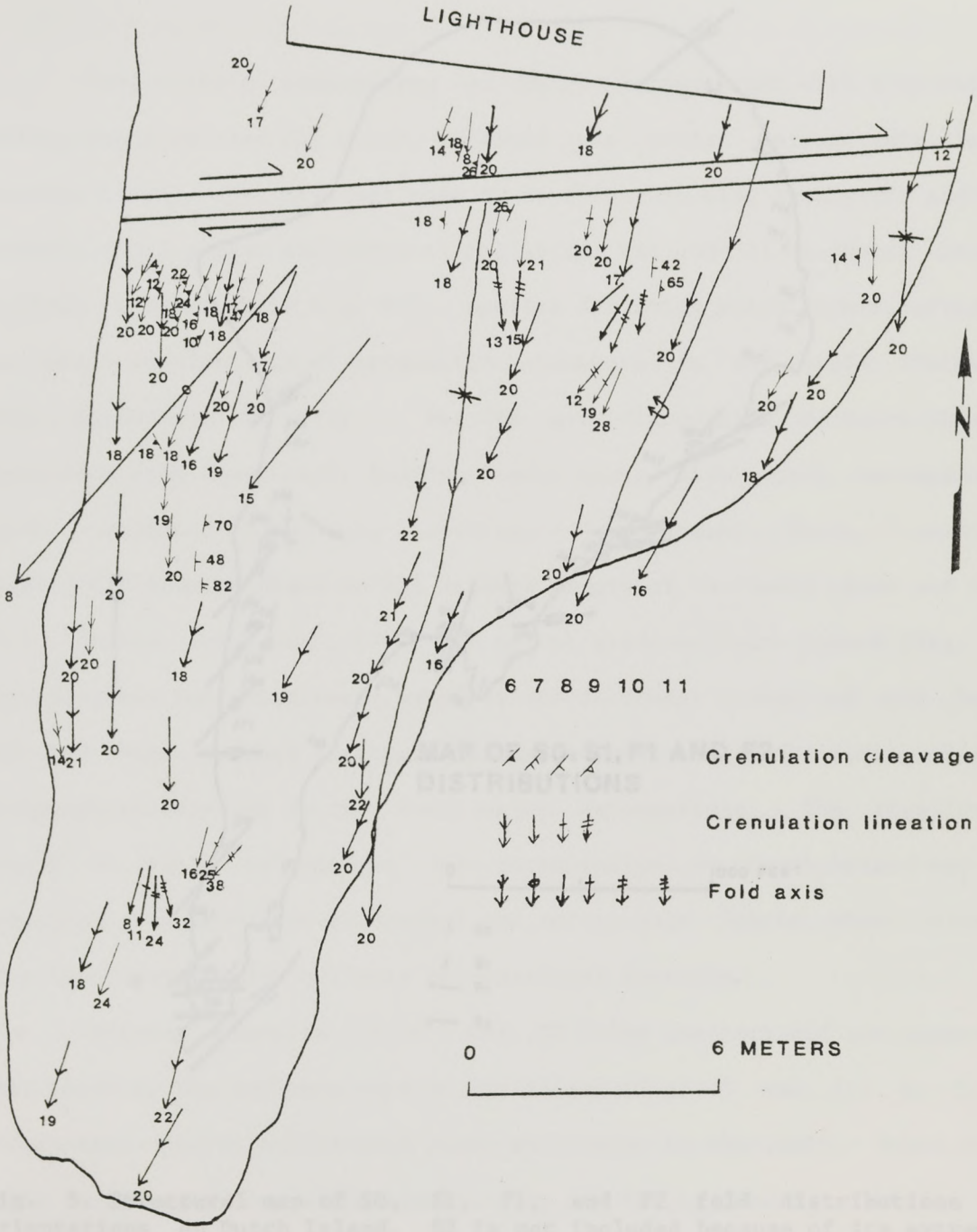


Fig. 4b. See Fig. 4a for description.

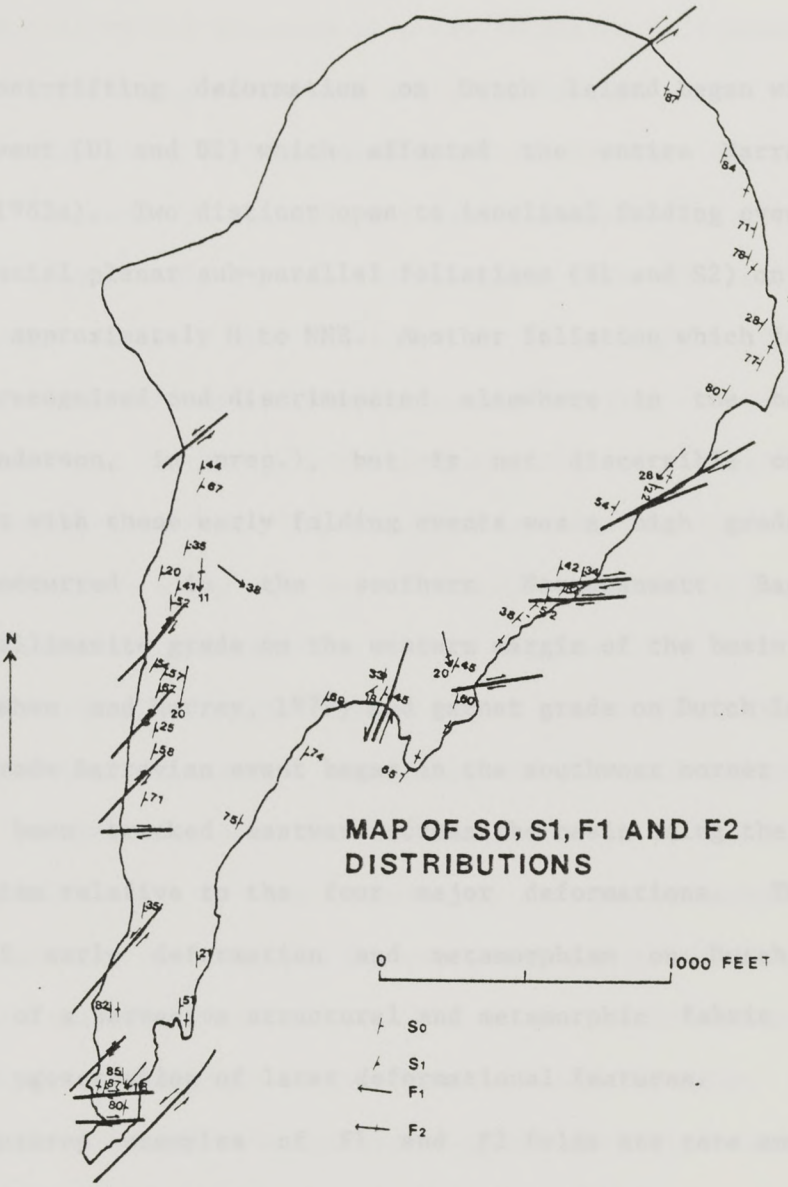


Fig. 5. Structural map of S0, S1, F1, and F2 fold distributions and orientations on Dutch Island. S2 is not included because of its extremely variable and pervasive character. Note that F1 and F2 folds are more common in the northern part of the island, where they have not been obliterated by later deformation. Strike-slip fault locations are shown for location reference only.

## EARLY DEFORMATION AND METAMORPHISM

Post-rifting deformation on Dutch Island began with a polyphase folding event (D1 and D2) which affected the entire Narragansett Basin (Mosher, 1983a). Two distinct open to isoclinal folding events (F1 and F2) produced axial planar sub-parallel foliations (S1 and S2) on Dutch Island striking approximately N to NNE. Another foliation which formed during D1 has been recognized and discriminated elsewhere in the basin (Farrens, 1982; Henderson, in prep.), but is not discernible on Dutch Island. Concurrent with these early folding events was a high grade metamorphism which occurred in the southern Narragansett Basin, reaching kyanite/sillimanite grade on the western margin of the basin (Grew and Day, 1972; Skehan and Murray, 1979) and garnet grade on Dutch Island (Fig. 1). This prograde Barrovian event began in the southwest corner of the basin and has been tracked eastward across the basin using the timing of peak metamorphism relative to the four major deformations. The significant result of early deformation and metamorphism on Dutch Island was the formation of a pervasive structural and metamorphic fabric which allowed excellent preservation of later deformational features.

Outcrop examples of F1 and F2 folds are rare and are generally restricted to the northern part of the island (Figs. 5 and 6), as later deformation partly obliterated these structures in the south. These folds verge in opposite directions elsewhere in the basin (Mosher, 1983a), but extreme reorientation of all early structures makes determination of original vergence directions for folds on Dutch Island impossible. Large scale F1 folds are somewhat more common than F2 folds and are generally of

greater magnitude. The two fold sets are differentiated by the folding of S1 by F2, and by the presence of a new foliation (S2) axial planar to F2. All of the early mesoscopic folds are tight to isoclinal.

The foliation (S2) produced by F2 is by far the most pervasive structural element on the island (see for example Figs. 9,10, and 11) and is readily identifiable in all lithologies with the exception of the metaquartzite units. The attitude of S2 is higly variable, due to the effects of later deformation, but generally strikes N to NNE. Outcrop measurements and localities for bedding (S0), S1, F1, and F2 are shown in Fig. 5. Strike-slip fault locations and orientations from Fig. 3 and the sense of motion along them are included in this and all other figures of this nature and are discussed in a later section.

The timing relations between D1, D2 and M1 (the first metamorphic event) and the structural complexity of the early deformation are best expressed in thin section. The S1 foliation is a complex metamorphic foliation as shown by its expression in the metaconglomerates. Some pressure solution features are observed, such as quartz tails growing off of larger quartzite cobbles parallel to the principle extensional strain (X), however, the interior of the cobbles show undulose extinction and significant subgrain development, suggesting higher strain conditions and/or higher temperatures (Nicolas and Poirier, 1976). The S1 foliation in the metapelites is defined by strongly aligned muscovite and biotite and is visibly transposed to form the crenulation cleavage S2 (Fig. 7a). The more penetrative S2 foliation is axial planar to microscopic F2 folds, and micas which formed during D1 are recrystallized in the S2 crenulation hinges. The S2 foliation wraps preexisting garnet porphyroblasts and

parallels quartz pressure shadows adjacent to the garnets (Fig. 7b). Quartz grains in the rocks show a number of deformation textures, including undulose extinction, basal and prism slip, subgrain growth and enhancement, grain boundary migration, and Boehm and Tuttle lamellae. Grains are generally elongate parallel to the S2 foliation and have undergone significant recrystallization, suggesting that the majority of quartz deformation occurred during D2 at elevated temperatures. Garnet-biotite geothermometry data collected for a suite of Dutch Island metapelites yielded a maximum metamorphic temperature of approximately 460 to 485 degrees Centigrade (Appendix I).

The change from pressure solution to ductile deformation during D1 and the growth of metamorphic minerals parallel to S1 indicates that metamorphism started during D1. In addition, relations between the S1 and S2 foliations and the garnet porphyroblasts (Fig. 7b) indicate that M1 culminated near the end of D1, prior to D2. Finally, the presence of pressure shadows off garnets parallel to S2, recrystallization of micas in S2 crenulation hinges, and quartz deformation textures show that temperatures were still elevated during D2, but were somewhat lower.

Biotite porphyroblasts define a lineation on the S1 surface which has been affected by all post-D2 deformation. This lineation is approximately normal to major left-lateral fault trends, and may be associated with the formation of the S1 foliation. However, the exact timing relations of the biotite lineation are uncertain and remain problematic.

Fig. 6. Field photo of isoclinal F1 fold in psammitic unit. Fold axis orientation is S20W, 35SW. The view is to the south.

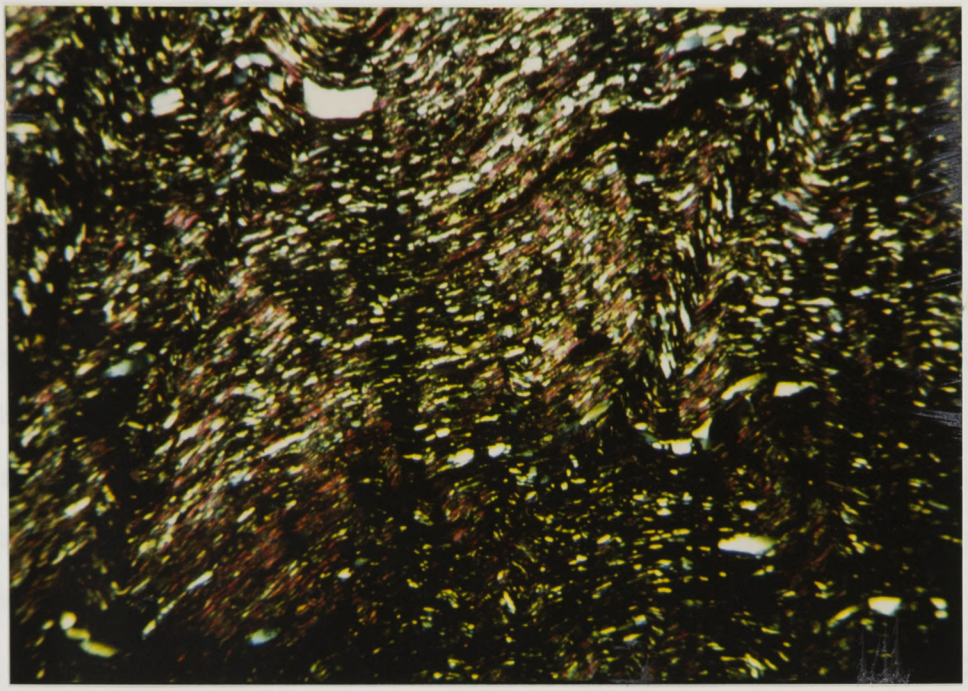

Fig. 7a. Photomicrograph showing the relation between S1 and S2. Here, S1 can be seen as a metamorphic mica foliation crenulated to form the S2 schistosity, as labelled on the photo.

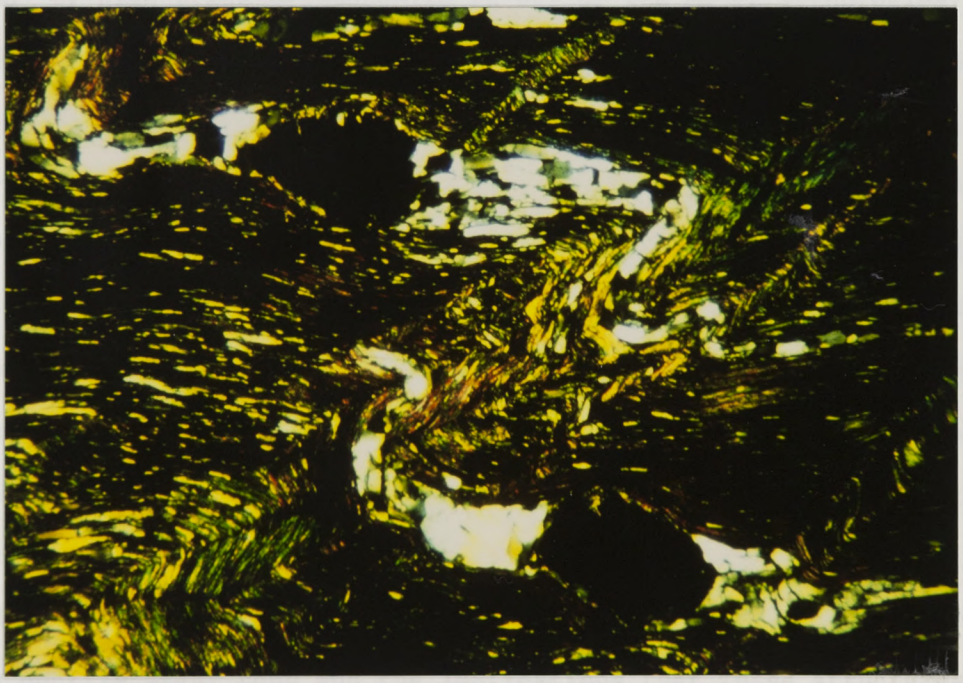

Fig. 7b. Photomicrograph of garnet porphyroblasts formed during M1. Quartz pressure tails are parallel to S2, and are affected by later shear-related crenulation cleavages. S1 is poorly expressed and is transposed parallel to S2 in this view. Note retrograde chloritization in this and other photomicrographs (scale for all photomicrographs is 1 inch = .3 cm).

A later retrograde metamorphic event (M2) is evident. Randomly oriented chlorite grains were found in all thin sections of Dutch Island rocks. Some chlorite grains are distinctly kinked, whereas other grains show no evidence of deformation. This variation in chlorite deformation textures indicates either that chloritization occurred both during and after shear-related deformation, or that the variation is due to a localizing effect of the D3 and D4 deformations. In either case, the retrograde metamorphism had no effect on the later structural development of Dutch Island.

The end result of the deformation produced during initial closure of the Narragansett Basin was the formation of a near-perfect foliation, enhanced by high grade metamorphism in all of the major lithologies. This foliation is not significant in itself, and can be found in greater or lesser degrees throughout the basin (Mosher, 1976; Skehan and Murray, 1979; Burks, 1981; Thomas, 1981; Farrens, 1982; Mosher, 1983a, 1983b). However, the presence of the foliation, combined with the generally fine-grained nature of the metasediments on Dutch Island, allowed remarkable preservation of later deformational events. Without the strong preexisting structural and metamorphic fabric preserved in the rocks, structures produced during later deformations would obliterate all earlier structures, and record only the most recent episode of significant deformation. The remainder of this study will focus on the types of structures produced in a complex ductile shear zone and the implications that these structures have on the strain and kinematic history of Dutch Island and the Narragansett Basin.

## SHEAR-RELATED DEFORMATION

The majority of deformation on Dutch Island may be attributed to discrete movement along a complex system of non-parallel, intersecting left-lateral and right-lateral strike-slip faults with approximately vertical fault planes. Structural superposition indicates that NNE- to NE-trending left lateral faults were first active, followed by right-lateral movement along predominantly NE- to ENE-trending faults. Some faults in NE orientations underwent both left-lateral and right-lateral movement, with left-lateral motion always preceding right-lateral motion (Fig. 3). Seven discrete fold sets were recognized and may be attributed to two progressive ductile shearing events on Dutch Island (D3 and D4). In addition, highly complex sets of discrete incremental crenulation cleavages generated by intersecting strike-slip faults were preserved and remained distinct after as much as 44 degrees of internal rotation. These structures will be discussed topically, first describing left-lateral deformation, then right lateral deformation, with additional sections describing crenulation cleavages, reoriented structures, and boudins.

### FAULTS

Discrete strike-slip faults and strike-slip fault zones (with widths varying from 5 to 20 meters and indeterminant lengths) were measured on Dutch Island in NNE to NE orientations with left-lateral motion and NE

to ENE orientations with right-lateral motion (Fig. 3). In addition to these measured faults, several other strike-slip faults may be readily inferred from outcrop patterns and topography. These fault localities, orientations, and movement histories corroborate fault movement data generated through geometric analyses of shear related folds on the island. Detailed study of outcrops along measured faults and of the areas between them has shown that the magnitude and intensity of deformation increases adjacent to the faults, although the overall style of deformation does not change. Within areas of fault intersection, the most intense deformation is observed, whereas areas that exhibit relatively little fault activity are the least intensely deformed. This variation allows extrapolation of fault locations based on deformation amplitude and intensity, and the orientations and movement histories of the faults can be inferred using structural superpositions and fold geometries. In outcrops which have undergone whole block rotation, the orientations of structures are different, but the internal geometries of the major fold sets are preserved, making possible restoration of the block's original position.

## FOLDS RELATED TO SHEARING

### LEFT-LATERAL FAULTING

Faults oriented NNE to NE with measurable left-lateral offset were mapped on Dutch Island. Reconstruction of fault orientations from fold geometries on the island also indicates left-lateral strike-slip faults

with these orientations (Fig. 8). Three distinctly different superposed fold sets (F5, F6, and F7) may be attributed to left-lateral strike-slip faulting, all of which formed due to episodic movement during a progressive deformation (fold sets F3 and F4 are preserved as highly reoriented structures and are discussed under separate heading). These folds young in a clockwise manner, and may be briefly characterized as follows:

F5 - N-S to S30W trending tight to open chevron folds plunging 8-25 degrees south. These folds may be upright, recumbent, or overturned, and have an average amplitude of 2-10 cm. (Fig. 9).

F6 - Open to tight recumbent folds trending generally S10W to S35W and plunging 5 to 20 degrees SSW. The folds verge eastward and range in amplitude from 15 cm. to >5 meters (Fig. 10).

F7 - Extremely broad, open folds trending S30W to S50W and plunging from 0 to 10 degrees SW. The axes of these folds are best defined by mapping reorientations in the trends of F5 and F6 (Fig. 11).

The field relationships between these fold sets are readily visible in outcrop at the south end of the island, where chevron folds (F5) are reoriented about the axis of a recumbent fold (F6) as shown in Fig. 12.


Fig. 8. Structural map showing locations of major F5, F6, and F7 folds, with strike slip fault locations and initial movement directions. Plunges of fold axes are indicated in degrees. Areas of extreme structural complexity (south end) show only representative structural data (see Fig. 4a and 4b for more detail). Fold styles and interrelations are described in text.

Fig. 9. Field photo of open F5 chevron folds. Orientation of fold axis is S12W, 14S with a westward vergence direction. Prominent schistosity is S2. View is to the SSW.

Fig. 10. Field photo of open, recumbant F6 fold. Orientation of fold axis is S20W, 20S with westward vergence. Note the younger fold (related to right-lateral shearing) parallel to the rapidograph cutting the hinge of the F6 fold. Prominent schistosity is S2. View is to the south.

Fig. 11. Field photo of large scale open F7 fold. Orientation of fold axis is S40W, 8SW and upright. The fold axis is defined by changes in orientation of F5 and F6 fold hinges (expressed in folds in cross sectional view as indicated on photo) and by the S2 schistosity. View is to the SW.

Fig. 12. Field photo showing the relation between F5 and F6, in which F5 chevron folds are visibly folded around the axis of a recumbant F6 fold. View is to the south.

Both of these fold sets are broadly warped about a south plunging F7 fold axis trending S40W (Fig. 11). Progressive tightening of limbs of earlier folds as well as consistent cross-cutting relations among these fold sets indicates that they are discrete folding events. The uniform clockwise younging directions of these folds and the small angle between fold sets suggest that successive folds formed and were then rotated in an anti-clockwise manner. This motion is consistent with what might be expected within a left-lateral shear couple which underwent progressive movement. Strain builds up along the shear plane, forming a generation of folds at an oblique angle to the mean shear plane. As movement occurs along the fault, the newly formed fold set will be rotated toward the kinematic a direction (Skjernaa, 1980; Ramsay, 1981) and thus closer to parallelism with the shear plane. As movement and subsequent rotation continues, the flattening strain within the X-Z plane tends to tighten the preexisting folds so that earlier fold sets have smaller inter-limb angles than younger folds. Structures of this nature may have formed within either a transpressional or a simple shear system, illustrated in Fig. 13. In this example, fold 1 forms within a left-lateral shear couple by flexural slip and is rotated and tightened until flexural slip can no longer occur. Fold 2 then forms at an angle to the shear plane, overprinting 1, which is now locked. Internal rotation of both 1 and 2 continues until 2 locks, at which point fold 3 is formed, overprinting both preexisting fold generations.

Stereonet representation of major and minor fold axes attributable to left-lateral shearing (Fig. 14a) shows that although fold orientations are variable depending on fault orientations, the internal geometry between

fold sets is consistent and usable for recognition and discrimination of discrete folding events. An average of 8 to 11 degrees of anticlockwise internal rotation was measured between F5 and F6, and 16 to 20 degrees of rotation between F6 and F7. Incremental fold orientation data for two left-lateral strike-slip faults are summarized in Fig. 14b. Note that progressively older fold sets exhibit a steepening in plunge, indicating a dip slip component along the faults. The presence of both vertical and horizontal slickensides within shear zones provides additional evidence for dip slip movement. Also, angles between the shear plane and individual fold sets show that F5 folds have been rotated approximately parallel to the shear plane, and that F7 folds are at about a 30 degree angle to that plane, suggesting that the folds may have formed at a slightly higher angle to the respective shear planes. The overall similarities of fold morphologies for individual fold sets may also suggest that strain rates along strike-slip faults were fairly homogeneous during this deformation despite marked differences in fault orientations.

## DEVELOPMENT OF INCREMENTAL FOLDS

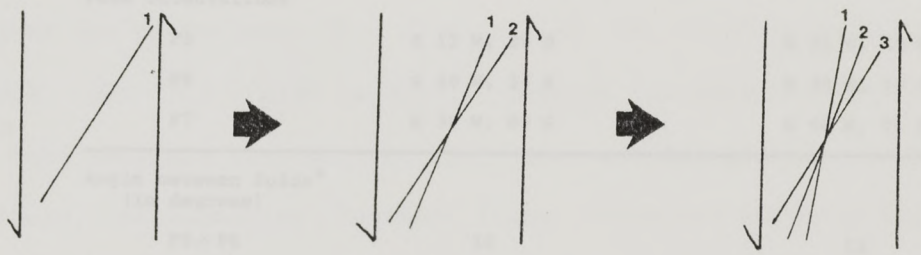


Fig. 13. Schematic diagram showing the development of incremental folds within a left-lateral simple shear system. Note the clockwise younging direction for progressive fold sets, indicating anticlockwise rotation.

a)

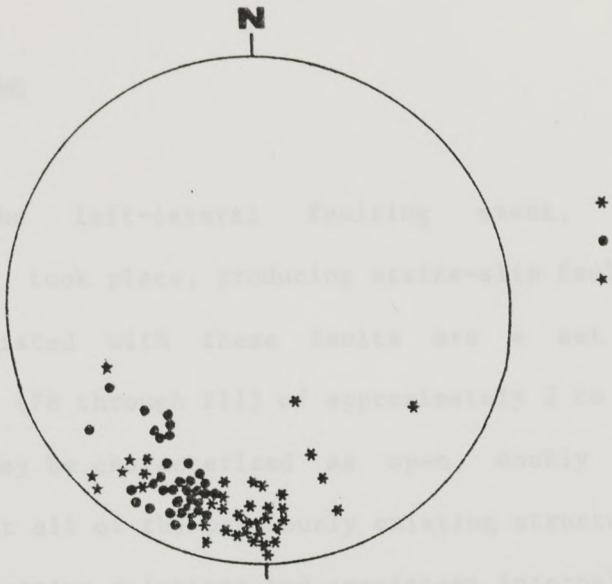


b)

| Fault Orientations | Fault 2 - N08E | Fault 3 - N20E |
|---|---|---|
| Fold Orientations* | | |
| F5 | S 12 W, 20 S | S 21 W, 14 S |
| F6 | S 20 W, 14 S | S 30 W, 10 S |
| F7 | S 38 W, 08 S | S 46 W, 06 S |
| Angle between folds* (in degrees) | | |
| F5 ∧ F6 | 10 | 11 |
| F6 ∧ F7 | 18 | 17 |
| F5 ∧ F7 | 28 | 30 |
| Angle between folds and shear plane | | |
| F5 | 4 | 1 |
| F6 | 12 | 10 |
| F7 | 30 | 26 |

*Note: All data are given as averages for measurements taken within 25 meters of the fault trace.

Fig. 14. Summary of left-lateral fold data and representative fault orientations (faults located on Fig. 8). a) Equal angular, lower hemisphere stereographic projection of F5, F6, and F7 fold data. Fold axes are labelled. Some scattering of fold axis orientations is observed, but individual fold sets maintain consistent internal geometries. b) Summary of average fold orientation measurements and rotational data for F5, F6, and F7 folds at left-lateral strike-slip faults in different orientations. Faults in NE orientations are not included because of the high degree of reorientation due to later right-lateral motion. Note that internal geometries between fold sets remain consistent between the two examples.

## RIGHT-LATERAL FAULTING

Following the left-lateral faulting event, a period of right-lateral shear took place, producing strike-slip faults in NE to ENE orientations. Associated with these faults are a set of mesoscopic crosscutting folds (F8 through F11) of approximately 2 to 5 cm amplitude. All of these folds may be characterized as open, doubly plunging folds which visibly affect all of the previously existing structures. The folds exhibit clear crosscutting relations and consistent internal geometries and young in an anticlockwise direction. The ranges of orientations for these fold axes are as follows: F8 - N38E to N51E, F9 - N18E to N28E, F10 - N08W to N02E, and F11 - N12W to N22W. Although the geometric relations among these fold sets are distinctive, they are morphologically very similar. The field relationships between these folds are shown in Fig. 15. The overall geometric consistency between all of the folds, which appear almost "ripple-like" or anastomosing in nature (Fig. 16), might make this deformation a likely candidate for progressive deformation due to inhomogeneous strain or lithologic variation. However, the clear and consistent overprinting relations that these folds display and the overall lithologic homogeneity of the Dutch Island phyllites seem to preclude this possibility. Instead, folds F8 through F11 represent incremental folds produced due to progressive deformation and subsequent rotation within a right-lateral shear couple. Thus, right-lateral fold sets formed sequentially at an angle to the mean shear plane, as did the left-lateral folds, and were rotated internally in a clockwise direction (Fig. 17).

Fig. 15. Field photo of F8, F9, F10, and F11 folds preserved on an S2 surface oriented S30W, 55SE. Fold generations are numbered as marked on photo. Note that folds young in a counterclockwise direction and that the angles between individual fold axes are small. View is to the west.

Fig. 16. Same as Fig. 15, except that folds in this outcrop have underwent 8 to 10 degrees of whole-block rotation from the outcrop in Fig. 15. Internal geometries are consistent throughout the island. View is to the west, and the photo was taken 10 meters north of Fig. 15.

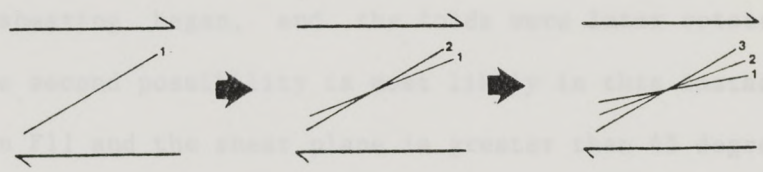


Fig. 17. Schematic diagram showing the development of incremental folds within a right-lateral simple shear system. Note the anticlockwise younging direction for progressive fold sets, indicating clockwise rotation.

Right-lateral fold and rotation data are summarized in a stereographic projection and a table (Fig. 19a and b) and indicate a swing in fold axis orientations between NE- and ENE-trending faults (Fig. 18). Adjacent to NE-trending faults, the angular relations between the folds and the shear planes are similar to those described for left-lateral shearing. However, along ENE-trending faults, the angles between respective right-lateral folds and the fault planes are markedly higher. Two possibilities could account for this difference: (1) less shearing has occurred along ENE faults than along NE faults, hence, angles between the folds formed due to shear and the fault plane are greater; (2) the NE shearing formed the folds before ENE shearing began, and the folds were later rotated during ENE shearing. The second possibility is most likely in this instance, as the angle between F11 and the shear plane is greater than 45 degrees, making a genetic relationship between these structures unlikely. In addition, there is no direct interference pattern among right-lateral fold sets at junctures between NE- and ENE-trending faults; rather, a gradual swing in fold axis orientation toward the ENE shear plane is observed, suggesting later reorientation. The plunges of folds F8 through F11 are relatively constant for progressively older folds indicating that, unlike D3, there was no significant dip slip component to the right lateral shearing event. The doubly plunging character of the right-lateral fold sets might be accounted for by lithologic inhomogeneity, variation within the strain field (Ramberg, 1964), or by the presence of a poorly developed fold set (F12) trending N65E, which cuts F8 through F11 at a high angle. The latter would give a doubly plunging appearance to these folds.

The degree of consistency of internal geometries for folds F8 through F11 (Fig. 19) allow discrimination of subtle changes in orientation of fold sets between outcrops. For example, the folds measured in the outcrop in Fig. 16 were 8 to 10 degrees anticlockwise from those same structures measured in an adjacent outcrop ten meters away. These measurements indicate that one of the outcrops was externally rotated (or rotated as a discrete block) 8 to 10 degrees after ductile deformation producing the fold sets had occurred. Elsewhere other rotated blocks can be identified using changes in fold axis orientations.

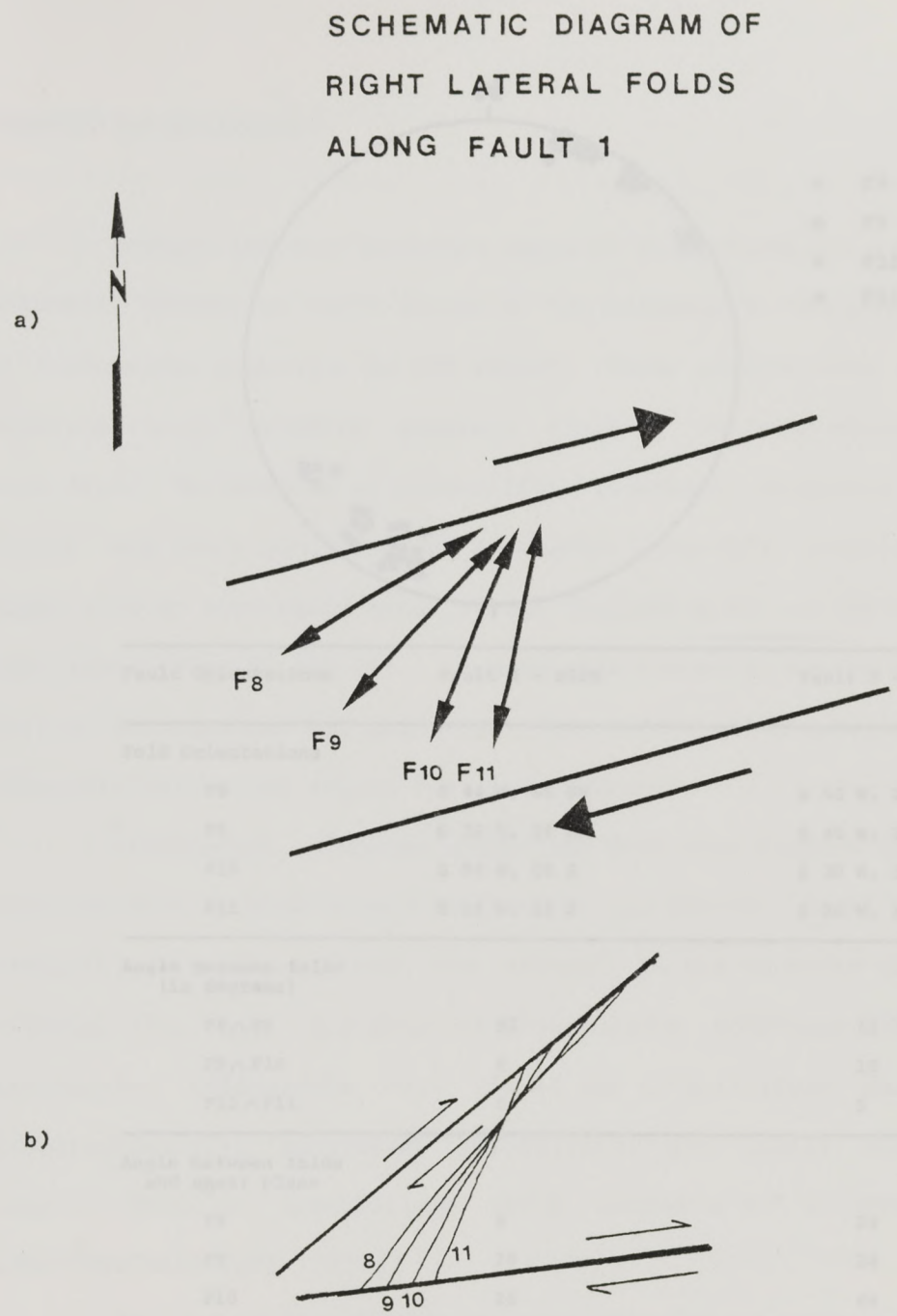


Fig. 18. (a) Close-up schematic diagram of right-lateral folds adjacent to Fault 1 in Fig. 3 (trending N74E). Fold measurements were taken on an S2 plane oriented approximately S70W, 14SE. Plunge data was negligibly different, varying from 4-16 degrees south and 4-7 degrees north on doubly plunging folds. (b) Schematic illustration showing the swing of fold axis orientations between NE- and ENE-trending faults.

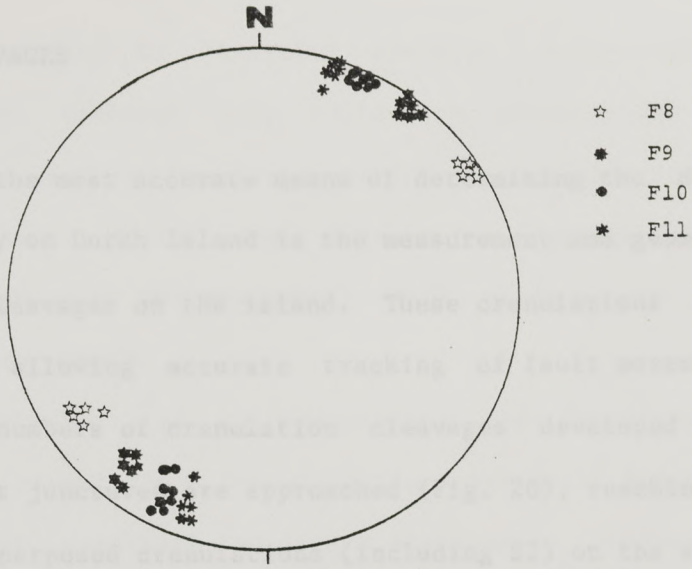


| Fault Orientations | Fault 4 - N52E | Fault 5 - N74E |
|---|---|---|
| **Fold Orientations** | | |
| F8 | S 44 W, 06 SW | S 50 W, 04 SW |
| F9 | S 32 W, 09 SW | S 40 W, 10 SW |
| F10 | S 24 W, 08 S | S 30 W, 12 S |
| F11 | S 18 W, 14 S | S 25 W, 10 S |
| **Angle between folds (in degrees)** | | |
| F8 ∧ F9 | 12 | 12 |
| F9 ∧ F10 | 8 | 10 |
| F10 ∧ F11 | 6 | 5 |
| **Angle between folds and shear plane** | | |
| F8 | 8 | 24 |
| F9 | 20 | 34 |
| F10 | 26 | 44 |
| F11 | 32 | 49 |

Fig. 19. Summary of right-lateral fold and rotation data for folds related to right-lateral shearing. a) Equal-angle, lower hemisphere stereographic projection of F8, F10, and F11 fold data rotated to a horizontal surface. Note the consistency of fold orientations. Fold axes are labelled. b) Table of right-lateral fold orientation data collected along two right-lateral faults. Note that internal geometries between fold sets are consistent, and that the angular relations between the folds and the adjacent faults are different (see text).

CRENULATION CLEAVAGES

Perhaps the most accurate means of determining the detailed fault movement history on Dutch Island is the measurement and geometric analysis of crenulation cleavages on the island. These crenulations exhibit clear superpositions, allowing accurate tracking of fault movement directions with time. The numbers of crenulation cleavages developed increases as faults and fault junctures are approached (Fig. 20), reaching a maximum of eight sets of superposed crenulations (including S2) on the southern end of the island (Fig. 4a and 4b). Even in this instance, overprinting relations between crenulations are consistent, and individual cleavages can be traced laterally across the island for tens of meters.

Crenulation cleavage geometries were also studied in oriented thin sections from samples taken from both in and between fault zones Clear crenulation superpositions are evident in the majority of thin sections examined (Fig. 21). All sets of crenulation cleavages associated with strike-slip deformation fold the S1 and S2 foliations, and major sets of crenulations with consistent orientations are easily discernible from locally produced crenulations which nucleated off of preexisting garnet porphyroblasts (Fig. 22).

The use of crenulation cleavage data for the structural analysis of Dutch Island proved most useful in areas of limited or poor quality outcrop. A large amount of data could be collected in a relatively small area, and the statistical dependability of crenulation internal geometries allowed for structural interpretation of sporadic outcrop along heavily vegetated or otherwise unexposed fault traces. Over 100 oriented thin

sections were studied to determine specific morphologies for the crenulation sets, although only collective orientations of groups of crenulations were used for predicting strike-slip fault orientations and movement directions. In all cases, crenulation cleavage data corroborated fault motions documented by mesoscopic fold orientations or by actual displacement measurements.

The technique for differentiating and discriminating between multiple sets of crenulations formed during progressive deformation is much the same as was described for larger structures. In short, a clockwise younging direction in a set of crenulation cleavages indicates anti-clockwise internal rotation and left-lateral shear. Conversely, anti-clockwise younging directions of crenulations indicate clockwise internal rotation and right-lateral shear. The orientations of the youngest cleavages, combined with the principle that rotated structures may approach but not lie parallel to the fault plane, help determine the orientation of the original shear plane. Angles between superposed crenulation sets, and orientations of crenulation cleavages relative to strike-slip fault orientations are summarized in Table 1.

Geometric analysis of Dutch Island crenulations indicate the following about strike-slip fault movement on Dutch Island:

- NNE- to NE-trending strike-slip faults show a left-lateral shear sense.

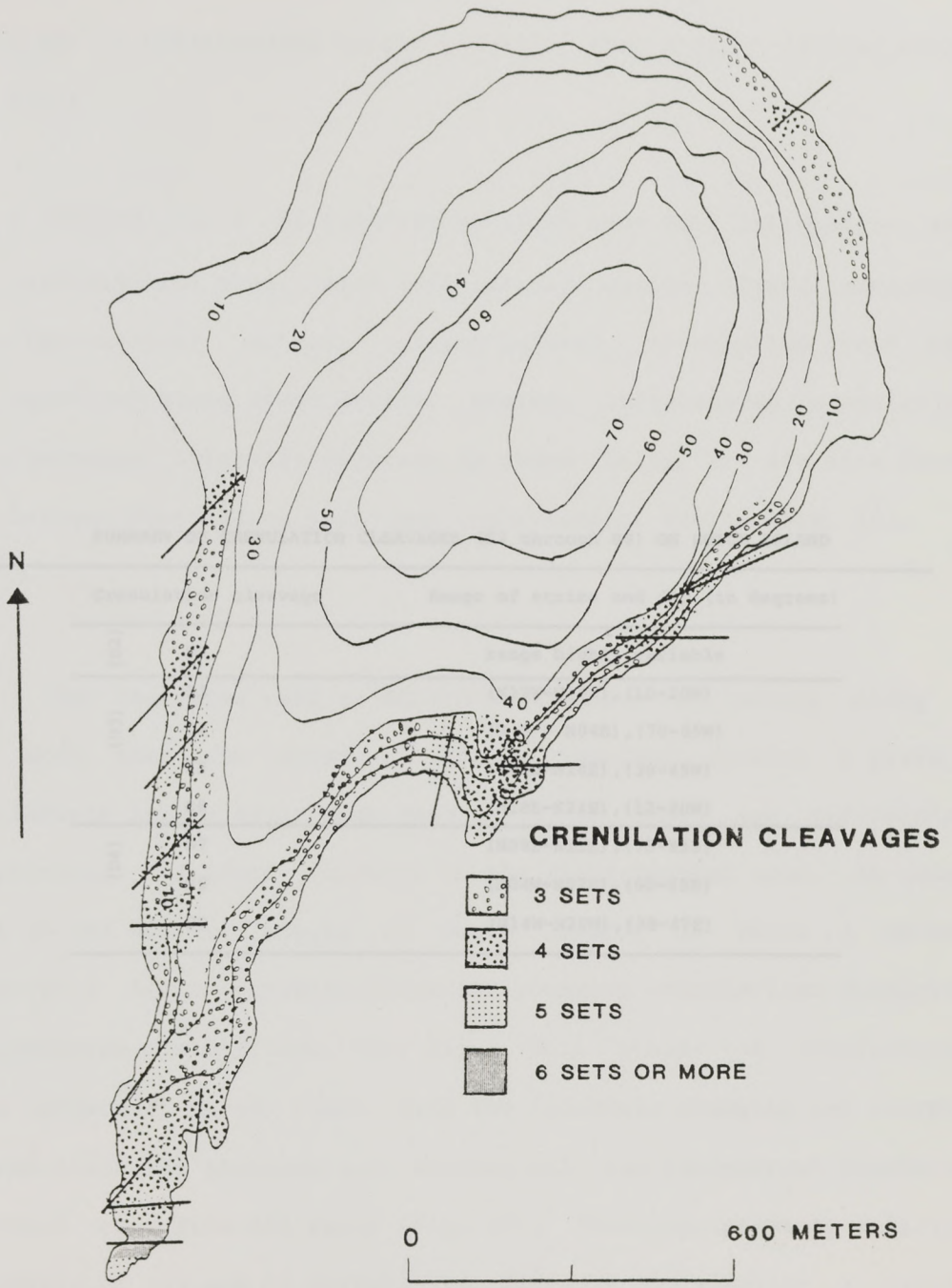


Fig. 20. Map of crenulation intensity on Dutch Island. The total number of crenulation sets developed are shown by hachure pattern. Note that the number of crenulation cleavages developed increases as faults and fault junctures are approached. A maximum of eight sets of superposed crenulations are developed at the southern end of the island (see Fig. 4a and 4b for detail).

SUMMARY OF CRENULATION CLEAVAGES (S2 through S8) ON DUTCH ISLAND

| Crenulation cleavage | | Range of strike and dip (in degrees) |
|---|---|---|
| (D2) | S2 | range highly variable |
| (D3) | S3 | (N22W-N18W),(10-20W) |
| | S4 | (N-S - N04E),(70-85W) |
| | S5 | (N08E-N14E),(30-45W) |
| | S6 | (N18E-N24E),(12-20W) |
| (D4) | S7 | (N08E-N11E),(75-85E) |
| | S8 | (N04W-N02E),(60-65E) |
| | S9 | (N14W-N20W),(38-47E) |

Table 1. Summary of average orientations for superposed crenulation cleavages on Dutch Island, rotated to a horizontal surface about a N-S axis. Angles between crenulation sets are indicated, within 4 degrees of variability. Note that cleavage planes generally decrease in dip in progressively older crenulations.

- NE- to ENE-trending faults generally show a right-lateral shear sense.

- Faults in a NE orientation often show both left-lateral and right-lateral shear, with left-lateral motion always preceding right-lateral motion. Right-lateral crenulation sets are localized along these faults, whereas left-lateral crenulation cleavages intensify adjacent to these faults, but are also found between NE-trending left- and right-lateral faults (Fig. 23).

The technique used to determine sequence of events along faults with more than one sense of motion involved tracing a given set of crenulations into a fault zone (map scale of 1:60) and determining the overprinting relations relative to the right-lateral sets. An example is found on the western margin of Dutch Island, in which a NE-trending strike-slip fault contains clockwise younging crenulations overprinted by anticlockwise crenulations (Fig. 24). Both groups of crenulations are found adjacent to the fault, with the clockwise younging set overprinting the anticlockwise younging set, whereas only the incremental clockwise set is found away from the fault (Fig. 23). These overprinting relations are an example of the use of crenulation cleavages to identify a strike-slip fault zone that underwent first left- and then right-lateral motion. Clockwise-younging crenulation cleavages formed during left-lateral shearing and were overprinted by anticlockwise-younging (right-lateral) crenulations localized adjacent to the fault plane. The intensity and

abundance of crenulation cleavages always increases adjacent to major strike-slip faults, varying from a minimum of three sets in relatively fault-free areas, to a maximum of eight sets at the junctures of left-lateral and right-lateral fault zones (Fig. 20). Crenulation cleavage data collected on Dutch Island show that right-lateral movement occurred after left-lateral motion on NE-trending faults, and that left-lateral movement on NNE-trending faults preceded right-lateral movement on both NE- and ENE-trending right-lateral faults.

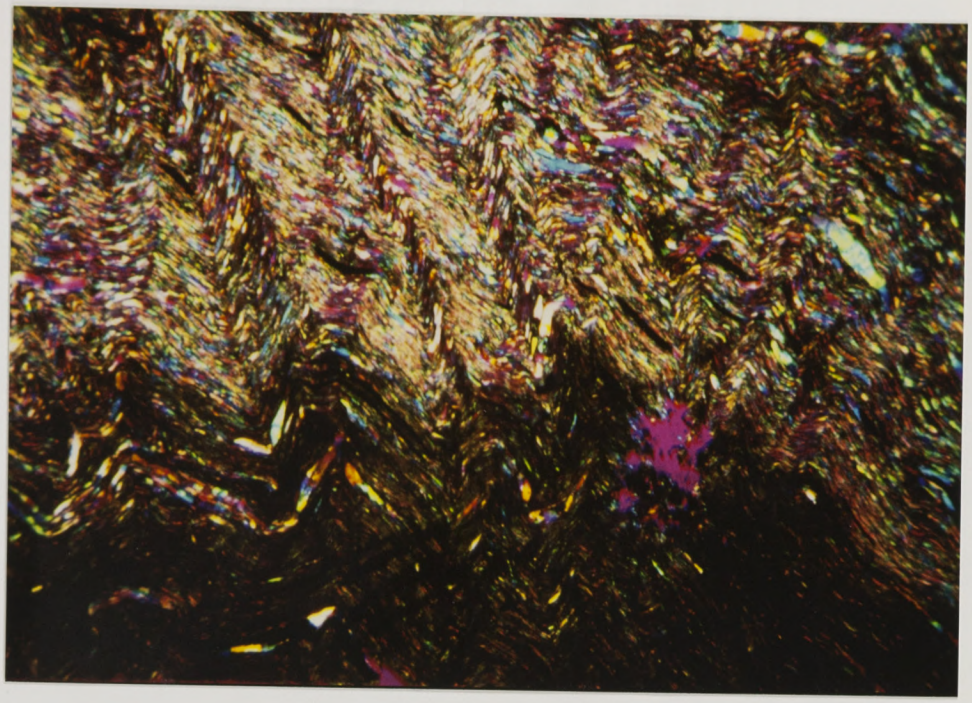

Fig. 21. Photomicrograph of discrete incremental crenulation cleavages on Dutch Island preserved in a phyllitic schist. Younging order is detailed in the sketch, based on crosscutting relations. View is cross-sectional normal to an S2 plane oriented N02E, 12E.

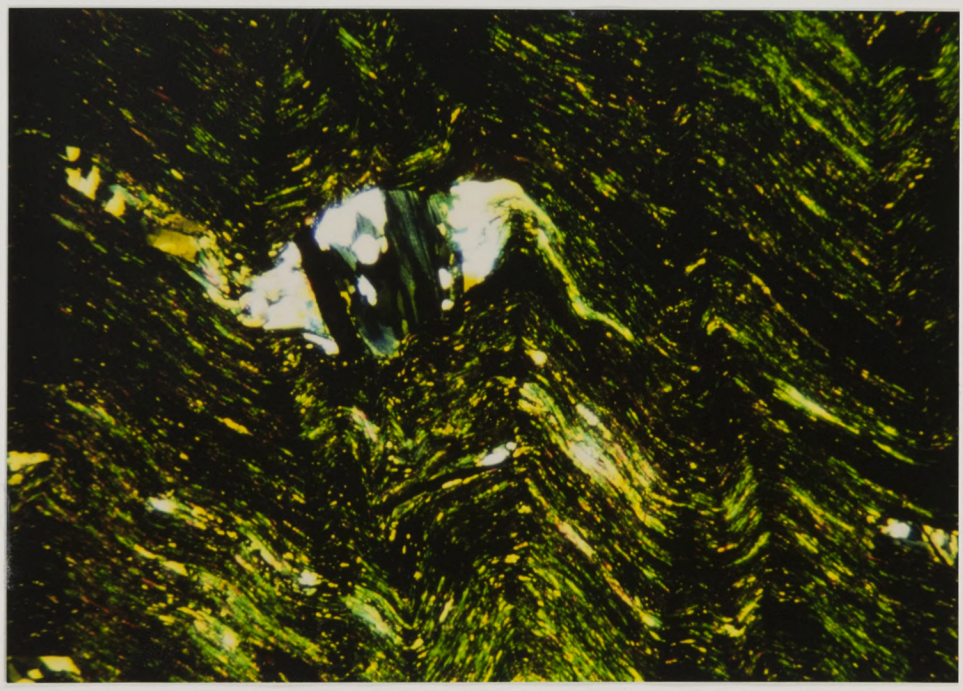

Fig. 22. Photomicrograph of anastomosing crenulation cleavages nucleating off of chloritized garnet porphyroblasts. There are no consistent crosscutting relations in crenulations such as these. View is cross-sectional normal to an S2 plane oriented N14W, 68W.

# INCREMENTAL CRENULATION CLEAVAGES ADJACENT TO STRIKE – SLIP FAULTS

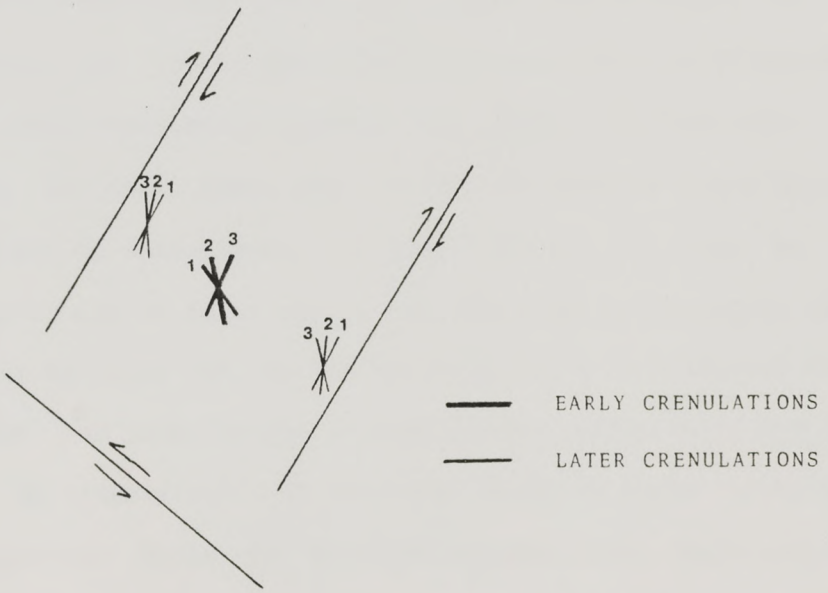


Fig. 23. Schematic diagram showing distributions of crenulation cleavages related to left- and right-lateral strike-slip faults. Note that left-lateral crenulations are found between right-lateral strike-slip faults, whereas right-lateral crenulations are localized along right-lateral faults. Overprinting relations are maintained in both instances.

Fig. 24. Field photo of superposed crenulation cleavages at a juncture between left- and right-lateral strike-slip faults. Individual crenulation cleavages are identifiable in 3 dimensions, but are most readily differentated in cross sectional view (see sketch). Numbers correspond to island-wide correlation sequence. View is to the south.

## OTHER FOLDING EVENTS

A number of outcrops on Dutch Island contain mesoscopic folds in orientations oblique to all major fold trends. These folds are found only in the coarser grained lithologies adjacent to strike-slip fault zones and have no associated axial planar cleavage or foliation. The folds are found in two general orientations adjacent to left-lateral faults which range in strike from N18E to N27E: S60E and plunging about 78 degrees to the SE (Fig. 25), and S30E and plunging up to 46 degrees to the south (Fig. 26), and are called F3 and F4, respectively (no chronologic order implied). The origin and later deformational history of these folds remains unknown. One possibility is that these folds are reoriented remnants of a discrete folding event or events that occurred between D2 and D3 which may or may not have been reoriented during the later deformations. A second possibility is that they are F1, F2, or early F5 folds which have been reoriented due to later shear. Of these choices, F1 must be ruled out, because the F3 and F4 folds appear to affect the S1 foliation (but not S2). F5 must also be ruled out, as the F5 folds are at a clockwise angle to the shear plane and rotation due to left-lateral shear could not rotate these folds to a SE orientation. On the other hand, F2 folds, found elsewhere in the Narragansett Basin in N to NNW orientations, could rotate into a SE orientation. The preexisting F2 folds would be rotated toward the kinematic a direction, however the steep plunges require both dip slip and strike-slip movement on these faults. The combined rotations would cause reorientation into SE orientations and abnormally steep plunges. Field measurements of slickensides on strike-slip fault planes show that a

considerable dip slip component was present on most faults, and the increase in plunge for the left-lateral fold sets also suggests possible dip slip movement. The direction of plunge for F3 and F4 indicates that the east side of the NNE-trending fault moved down with respect to the west side. The schematic diagram in Fig. 27 shows how a preexisting fold at an oblique angle to the shear plane would be rotated within a left-lateral shear system with a dip slip component (as described above) toward the shear plane (or the kinematic a direction) and increase in plunge. The end result would produce folds at a high angle to the major structural trends, which were preserved in anomalous orientations dependent on the amount of original deviation from horizontality of the axial planes or on the magnitude of the dip slip component along the fault.

Fig. 25. Field photo of F3 fold trending S12E, 78SE adjacent to a left-lateral fault bearing N27E. View is to the south.

Fig. 26. Field photo of F4 fold trending S30E, 43SE adjacent to a left-lateral fault trending N27E. Photo was taken 1 meter west of photo in Fig. 26. View is to the SE.

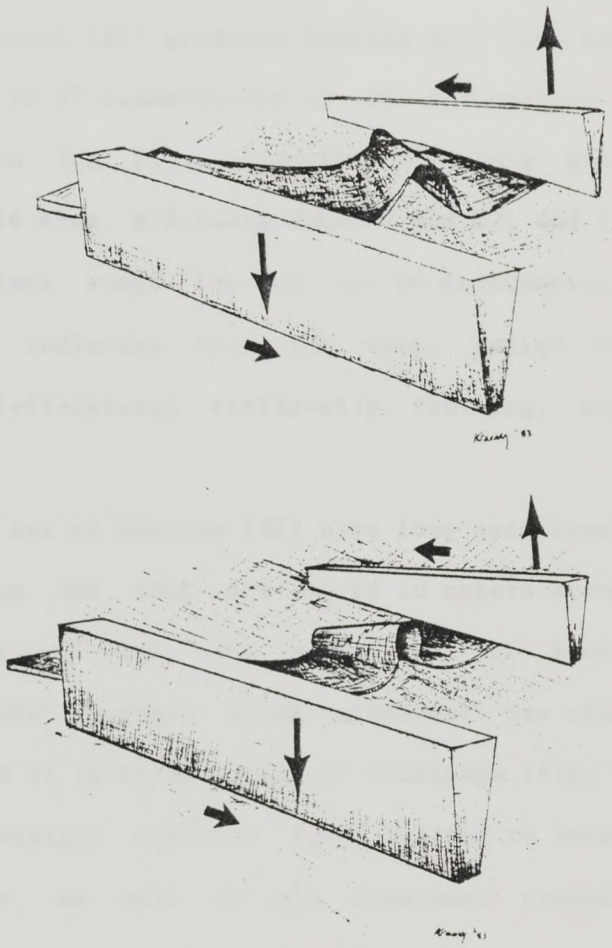

Fig. 27. Schematic diagram showing progressive rotation of a fold toward the kinematic a direction and an increase in plunge due to shearing with a dip slip component. The shear couple is left-lateral, trending NNE with an west-over-east dip slip component.

## BOUDINAGE

Two distinct sets of boudins were mapped on Dutch Island in this study. The first event (B1) produced boudins with long axes trending N and extension parallel to S2 (subtraction of D4 deformation indicates an E extension direction for B1). Examples of these structures are found throughout the field area, affecting both S1 and S2, and the boudins were folded by both late stage D3 and all D4 deformation. The timing and orientation of B1 indicates that the first period of boudinage was associated with left-lateral strike-slip faulting, and occurred early during D3.

The second set of boudins (B2) have long axes trending E with a N extension direction and they are up to 10 meters across between boudin necks in cross-sectional view. The second set of boudins erode to a curious "dimple-like" pattern along prominent sea cliffs which allowed clear determination of relative timing of boudinage (Fig. 28). The second set of boudins visibly affected folds related to both left-lateral and right-lateral shear, as well as all prominent crenulation cleavages. However, the extension direction for B2 is appropriate for right-lateral shear, suggesting that the boudinage was a late phase of the D4 deformation. Some of the boudins show evidence of additional later extension along an E-trending axis in which opening occurred along two planes, the first dipping south at about 45 degrees and the second dipping north at about 45 degrees. This last phase of boudinage-type deformation first opened north over south, and then later south over north within an E-trending right-lateral shear couple, indicating a change in strain

orientation during right-lateral shearing. A detailed analysis of boudinage was not conducted, aside from the basic boudin geometries mentioned above.

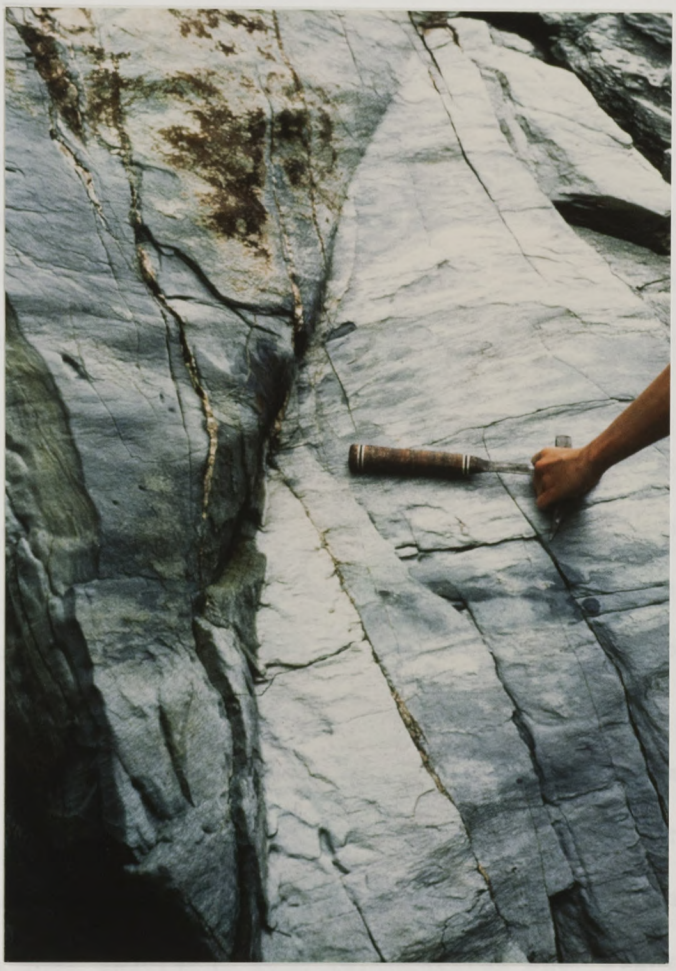

Fig. 28. Field photo showing weathering profile of boudins on Dutch Island. Note that the boudin neck affects folds produced during right-lateral shear, indicating that the second episode of boudinage occurred after F11. The prominent foliation is S2. View is to the west.

# DISCUSSION

The complex structure found on Dutch Island was formed as a result of complex movement along a system of non-parallel strike-slip faults, overprinting a strong metamorphic and structural fabric developed during initial basin closure. Considerable amounts of whole block rotation measured in discrete blocks around the island suggest that the island as a whole may have acted as a large block caught up and rotated in a complex fault system. Clearly, a question remains as to the regional significance of a locally complicated structural problem. The fault trends and movement directions must be present away from the island in order to extrapolate strain history information to the Narragansett Basin at large. If the major fault orientations observed on Dutch Island are not unique within the basin, then a detailed structural analysis of the island would help to determine the large-scale strains that were acting on the basin during late stage deformation.

The strike-slip fault orientations and motions measured on Dutch Island may be summarized as follows: left-lateral strike-slip faults generally trend NNE to NE, right-lateral strike-slip faults trend NE to ENE, and faults that underwent both left-lateral and right-lateral motion are oriented NE. For the latter case, left-lateral movement always preceded right-lateral movement. Consistent internal geometries between individual fold sets associated with both left-lateral and right-lateral faults, as well as clear-cut relations between the shear plane orientations and fold axis orientations for left-lateral folds made accurate restoration

of inferred fault orientations and movement histories possible on Dutch Island.

In response to shearing, folds apparently initiate at angles slightly greater than 30 degrees to the shear plane and rotate towards the kinematic a direction. At least 26 degrees of internal rotation of mesoscopic folds and crenulation cleavages occurred adjacent to both left- and right-lateral faults. Fold rotation toward the shear plane continues until the fold can no longer accomodate the flattening strain and locks up. A new fold set then forms at approximately 30 degrees to the shear plane and overprints the earlier (and presently locked) sets. Between 6 and 18 degrees of internal rotation can occur prior to initiation of a new set of folds. In addition, as much as 10 degrees of external, whole block, clockwise rotation (right-lateral motion) affected structures on the island. Steepening of progressively older fold sets associated with left-lateral strike-slip faults is most likely attributable to a dip slip component, in which the east side of the fault moved down with respect to the west side. Folds generated by right-lateral faulting formed first due to NE shearing and were later reoriented by ENE faults. No significant dip slip movement was associated with right-lateral shearing.

A map of basin bathymetry around Dutch Island constructed by M.C. Henderson (Fig. 29), shows trends of topographic highs and lows on the basin floor around the island. These trends form lineations in the same general orientations as fault orientations mapped on Dutch Island, and often appear to be offshore extensions of structures measured on the island. This information, combined with gravity and magnetic data collected for the southern Narragansett Basin (Fig. 1), strongly indicate

that the fault trends observed on Dutch Island are present immediately adjacent to the island, as well as in outcrop elsewhere in the basin (Skehan and Murray, 1979; Burks, 1981; Mosher, 1983a; Henderson, in prep.). A composite map of faults on Dutch Island and faults inferred from basin topography and geophysical data (Fig. 29) presents an overview of faulting on and around the island. A major N- to NNE-trending left-lateral shear zone bends and splays immediately south of Dutch Island. The subsidiary faults formed at the splay could account for the extreme structural complexity in the southern part of the island. Other major lineaments surrounding the island are similar in orientation to mapped faults on land, suggesting possible offshore counterparts, if not extensions, of these faults. The fault pattern observed on Dutch Island could allow for some whole block rotation in the southern part of the island, although similarities in fold and fault orientations around the island would preclude any significant rotation on greater than outcrop scale.

The large amount of strike-slip deformation observed on Dutch Island and elsewhere in the Narragansett Basin suggest that the fault patterns on the island may fit within the tectonic framework of a left- or right-lateral megashear system, active in the late Paleozoic. Relative motions and orientations of the faults on Dutch Island could be analogous to R and R′ riedel shears within a larger shear zone. These shears could fit in either of two possible strain ellipse configurations: elongate in a NNE manner parallel to a left-lateral shear zone, or elongate in an E-W orientation parallel to a dextral shear zone ( Fig. 30a). Either of these shear systems could produce strike-slip faults that trend NNE with left-lateral motion and ENE with right-lateral motion (Fig. 30b).

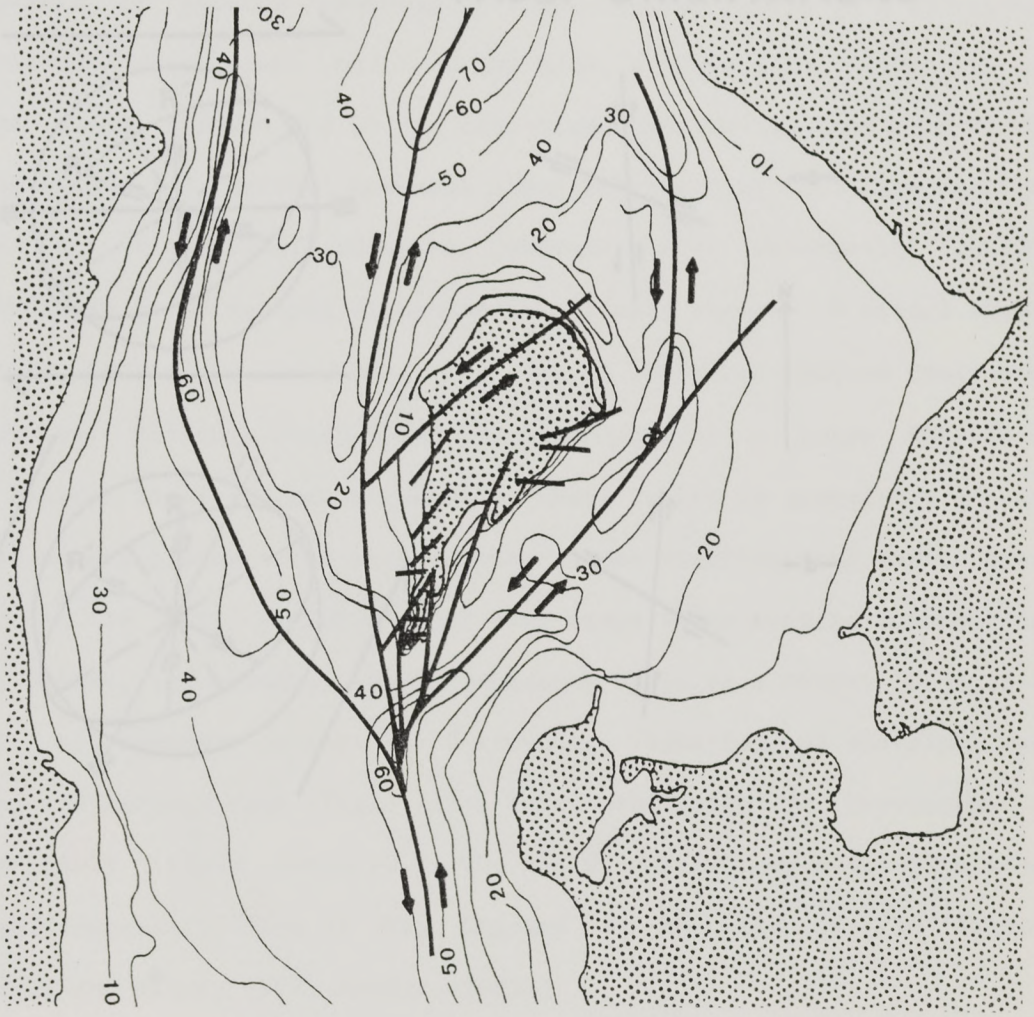


Fig. 29. Composite map of basin bathymetry (after Henderson, in prep.) showing depths to basin floor in feet and known and inferred faults on and around Dutch Island. Note prominant linear lows around Dutch Island, corresponding to major strike-slip fault localities, and the complex splay system in the southernmost part of the island, producing both right- and left-lateral strike-slip faults

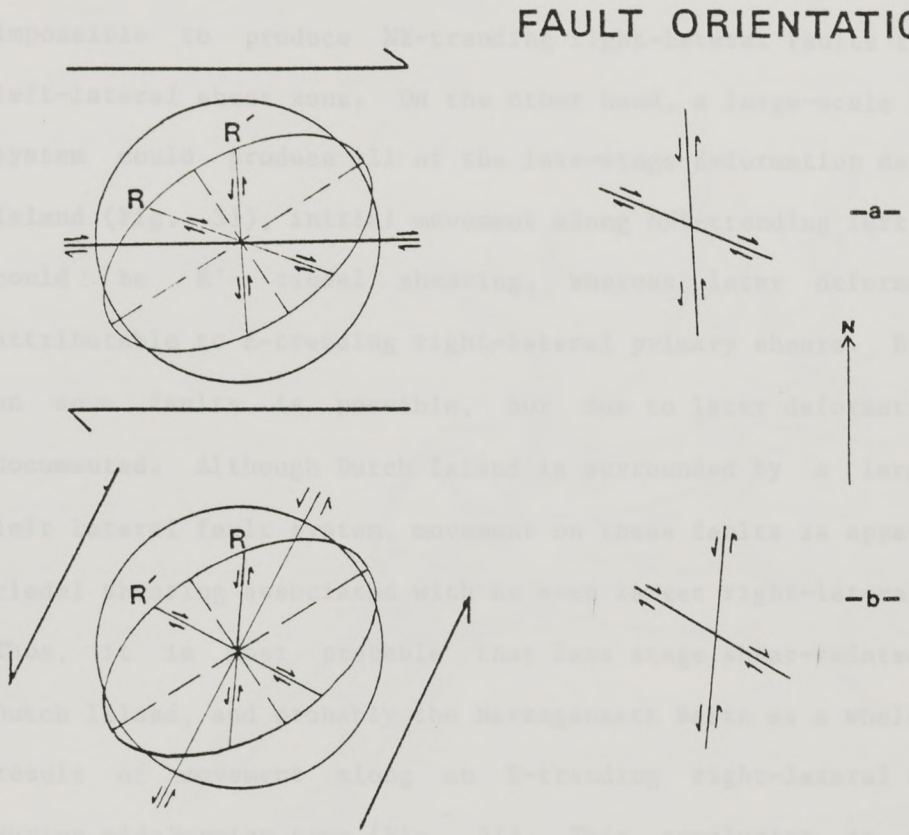


Fig. 30. Schematic figure showing possible orientations for large-scale shear systems which would produce R and R′ riedel shears in feasible orientations for modelling deformation mechanisms on Dutch Island. Model (*a*) is more likely to be correct, as NE-trending right-lateral faults would be very difficult to produce in model (*b*), and fault movement is not concurrent.

However, the NNE-trending faults and the ENE-trending faults are not concurrent, and so should not be riedel shears. Additionally, it would be impossible to produce NE-trending right-lateral faults in a NNE-trending left-lateral shear zone. On the other hand, a large-scale E-trending shear system could produce all of the late-stage deformation described on Dutch Island (Fig. 31); initial movement along NNE-trending left lateral faults could be R′ riedel shearing, whereas later deformation would be attributable to E-trending right-lateral primary shears. R riedel shearing on some faults is possible, but due to later deformation could not be documented. Although Dutch Island is surrounded by a large NNE-trending left lateral fault system, movement on these faults is apparently due to R′ riedel shearing associated with an even larger right-lateral fault system. Thus, it is most probable that late stage shear-related deformation on Dutch Island, and probably the Narragansett Basin as a whole, occurred as a result of movement along an E-trending right-lateral transform system during mid-Permian time (Fig. 31). This conclusion is consistent with major fault trends elsewhere in the basin, and is compatible with several tectonic reconstructions of New England at the end of the Paleozoic (Arthaud and Matte, 1977; Mosher, 1983b).

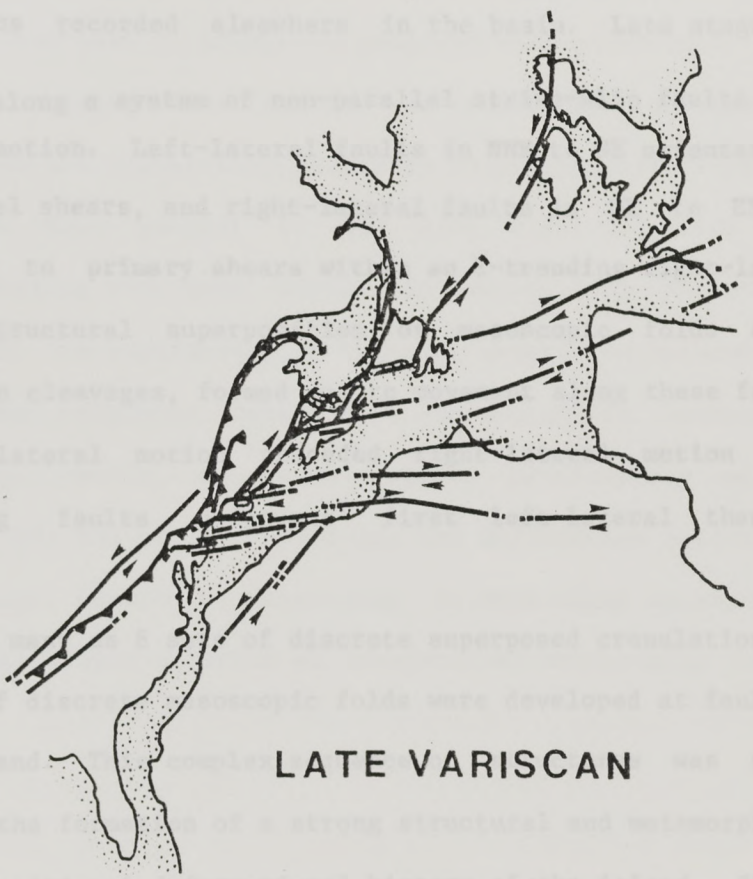


Fig. 31. Paleogeographic reconstruction of New England during the late Variscan, showing locations and movement directions of major transform systems active during the Devonian until the end of the Permian. The model proposed for late-stage deformation on Dutch Island and for the Narragansett Basin is compatible with this reconstruction. After Arthaud and Matte (1977).

# CONCLUSIONS

The deformation on Dutch Island is the most intense and complex structure observed in the Narragansett Basin. Four major deformational events were preserved in the metasediments, corresponding to the four major deformations recorded elsewhere in the basin. Late stage deformation is localized along a system of non-parallel strike-slip faults with opposite senses of motion. Left-lateral faults in NNE to NE orientations correspond to R´ riedel shears, and right-lateral faults in NE to ENE orientations correspond to primary shears within an E-trending right-lateral transform system. Structural superposition of mesoscopic folds and incremental crenulation cleavages, formed due to movement along these faults, indicates that left-lateral motion preceded right-lateral motion and that many NE-trending faults underwent first left-lateral then right-lateral movement.

As many as 8 sets of discrete superposed crenulation cleavages and 7 sets of discrete mesoscopic folds were developed at fault intersections on the island. This complex sequence of structures was preserved as a result of the formation of a strong structural and metamorphic fabric early in the depositional deformational history of the island. Study of geometry and overprinting relations of the fold and crenulation sets within adjacent shear zones served to track movement along individual faults through time.

Structural analysis of the complex deformation on Dutch Island indicates that accurate tracking of fault motion within complex shear systems is feasible in areas in which overprinting relations between progressive deformations are preserved. In addition to the regional

significance of the study, the following observations were made: (1) folds related to left- and right-lateral strike-slip faulting on Dutch Island formed at approximately 30 degrees to the shear plane, and the earliest folds were subsequently rotated approximately parallel to the mean shear plane; (2) increase in plunge of progressively older fold sets associated with left lateral faulting may be attributed in part to a dip slip component to the strike-slip faults in which the east side of the fault moved down with respect to the west side, (3) folds related to right lateral shearing were most useful in determining whole-block rotations because of the consistency of internal geometries between fold sets;; (4) deformational intensity, complexity, and amplitude increase adjacent to strike-slip faults on Dutch Island, particularly at complex fault junctures; (5) the structural styles and deformation patterns described on Dutch Island should be analogous to what might be expected in a larger block caught within a system of non-parallel strike-slip faults.

# APPENDIX I

## GARNET ZONATION CHARACTERISTICS AND GARNET - BIOTITE GEOTHERMOMETRY

### INTRODUCTION

Euhedral garnets which formed during the early prograde metamorphism of Dutch Island were chemically analyzed by electron microprobe as a part of this study in order to determine compositional zoning profiles. Additionally, garnet and primary biotite were found in grain-to-grain contact, allowing the application of a garnet-biotite geothermometry technique to a number of samples.

Two microprobe sections were cut from samples in the phyllite lithology, they contained the assemblage quartz + muscovite + biotite + garnet + ilmenite + graphite, with retrograde chlorite and sphene. These sections were selected for analysis because they contained a minimal amount of chloritized garnet and contained garnet and biotite grains in intimate contact. For each garnet, compositions were determined along a rim-core-rim traverse at wiht analysis points spaced 25 microns apart. Data were obtained using a combination of energy-dispersive and wavelength-dispersive techniques, yielding weight percents of oxides of eight major and minor elements: Fe, Mg, Mn, Si, Al, K, Ca, and Ti.

COMPOSITIONAL ZONING DATA

The relative abundances of Fe, Mn, and Mg are of critical importance in determining garnet zoning and composition. For this reason, these elements were analyzed using the wavelength-dispersive spectrometers. Abundances of Al, Si, K, Ca, and Ti were determined using energy-dispersive methods. For each analysis, the total weight percent of oxides was considered acceptable only in the range of 100+/-2 wt. percent for the garnets. Garnet compositional data are given in Tables 2a and 2b; average compositions are $Al_{77}Gr_{9}Sp_{11}Py_{3}$ (sample DI-5) and $Al_{67.1}$ $Gr_{16.2}$ $Sp_{12.7}$ $Py_{4.0}$ (sample DI-12a). The following are brief descriptions of the zoning charateristics of the two garnets:

DI-5. The garnet sampled in this section shows a general decrease in Mn and Ca from core to rim, and an increase in Fe, Mg, and Mg/Fe from core to rim. These data are summarized in a graphic traverse format in Figures 32a through 32d, with a ternary plot of Fe, Mg, and Mn showing mole fractions of all points analyzed (Fig. 33a).

DI-12a: This garnet shows a rather confusing and apparently random pattern of element zoning across the garnet, in which Mn and Ca rise and fall inversely compared to Fe, Mg, and Mg/Fe. This is conceivably the result of multiple nucleation of grains. Graphic representation of these data is inconclusive, but a plot

of data on a ternary diagram shows that zoning patterns are somewhat similar to those displayed by the garnet in DI-5 (Fig. 33b).

TABLE 2a

| | WEIGHT PERCENT OF OXIDES | | | | | RATIOS FROM MOLE FRACTIONS | | |
|---|---|---|---|---|---|---|---|---|
| Sample # | FeO | MgO | MnO | CaO | $Al_2O_3 + SiO_2$ | Ca/Fe | Mg/Fe | Mn/Fe |
| 1 | 33.3 | 1.3 | 4.0 | 4.5 | 56.4 | .18 | .07 | .12 |
| 2 | 32.0 | 0.7 | 7.0 | 3.3 | 57.0 | .14 | .04 | .22 |
| 3 | 31.4 | 0.6 | 6.4 | 3.3 | 58.1 | .14 | .04 | .21 |
| 4 | 32.8 | 0.5 | 7.0 | 4.0 | 55.8 | .16 | .03 | .22 |
| 5 | 34.7 | 1.6 | 2.1 | 2.8 | 59.0 | .20 | .08 | .06 |
| 6 | 32.6 | 1.4 | 4.4 | 3.1 | 58.5 | .12 | .07 | .14 |
| 7 | 33.0 | 1.4 | 4.0 | 3.3 | 58.5 | .13 | .07 | .12 |
| 8 | 34.3 | 1.5 | 3.0 | 3.2 | 58.0 | .12 | .08 | .09 |
| 9 | 34.0 | 1.5 | 2.7 | 3.3 | 58.5 | .13 | .07 | .12 |
| 10 | 30.0 | 1.1 | 5.1 | 3.7 | 60.0 | .15 | .07 | .18 |
| 11 | 30.1 | 1.1 | 6.0 | 3.7 | 58.5 | .15 | .07 | .19 |
| 12 | 32.9 | 1.3 | 3.6 | 3.3 | 58.8 | .13 | .07 | .11 |
| 13 | 32.6 | 1.8 | 2.0 | 2.5 | 61.0 | .10 | .10 | .06 |
| 14 | 31.0 | 1.2 | 5.2 | 3.6 | 59.0 | .15 | .07 | .17 |
| 15 | 32.2 | 1.2 | 4.3 | 3.5 | 58.7 | .14 | .07 | .14 |
| 16 | 31.9 | 1.3 | 4.3 | 3.4 | 59.2 | .13 | .07 | .14 |

TABLE 2b

| | WEIGHT PERCENT OF OXIDES | | | | | RATIOS FROM MOLE FRACTIONS | | |
|---|---|---|---|---|---|---|---|---|
| Sample # | FeO | MgO | MnO | CaO | $Al_2O_3 + SiO_2$ | Ca/Fe | Mg/Fe | Mn/Fe |
| 1 | 23.9 | 1.0 | 2.2 | 3.9 | 69.0 | .22 | .08 | .10 |
| 2 | 23.5 | 0.3 | 6.0 | 8.6 | 61.6 | .47 | .02 | .25 |
| 3 | 27.9 | 1.9 | 5.0 | 5.8 | 59.4 | .30 | .13 | .19 |
| 4 | 28.0 | 1.8 | 5.4 | 6.5 | 58.3 | .30 | .11 | .19 |
| 5 | 30.5 | 1.7 | 4.8 | 5.9 | 57.1 | .26 | .11 | .17 |
| 6 | 21.8 | 0.8 | 5.5 | 9.0 | 63.8 | .52 | .07 | .26 |
| 7 | 35.4 | 1.0 | 4.2 | 4.6 | 54.7 | .09 | .05 | .12 |
| 8 | 32.5 | 0.9 | 6.3 | 3.3 | 56.9 | .14 | .05 | .19 |
| 9 | 29.5 | 0.4 | 7.2 | 4.0 | 59.0 | .19 | .01 | .26 |
| 10 | 31.0 | 0.7 | 6.0 | 3.8 | 58.5 | .15 | .04 | .19 |
| 11 | 33.4 | 0.8 | 6.7 | 3.3 | 55.8 | .13 | .04 | .20 |
| 12 | 29.7 | 0.6 | 4.8 | 6.3 | 58.6 | .26 | .04 | .16 |
| 13 | 30.0 | 0.5 | 5.3 | 6.7 | 57.5 | .28 | .03 | .18 |

Table 2. Tabulated data accumulated for garnets DI-5 (a) and DI-12a (b).

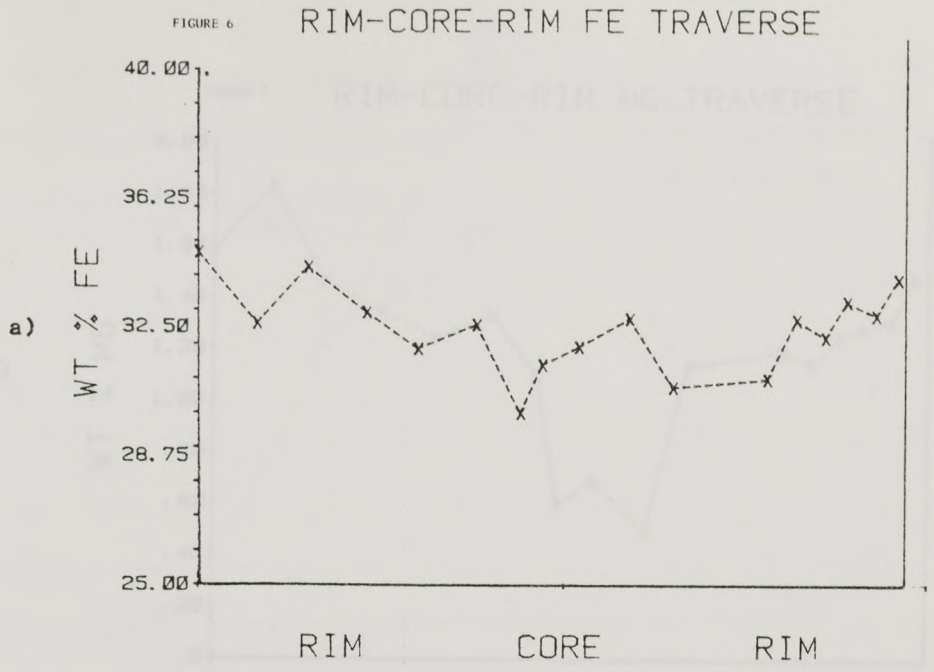


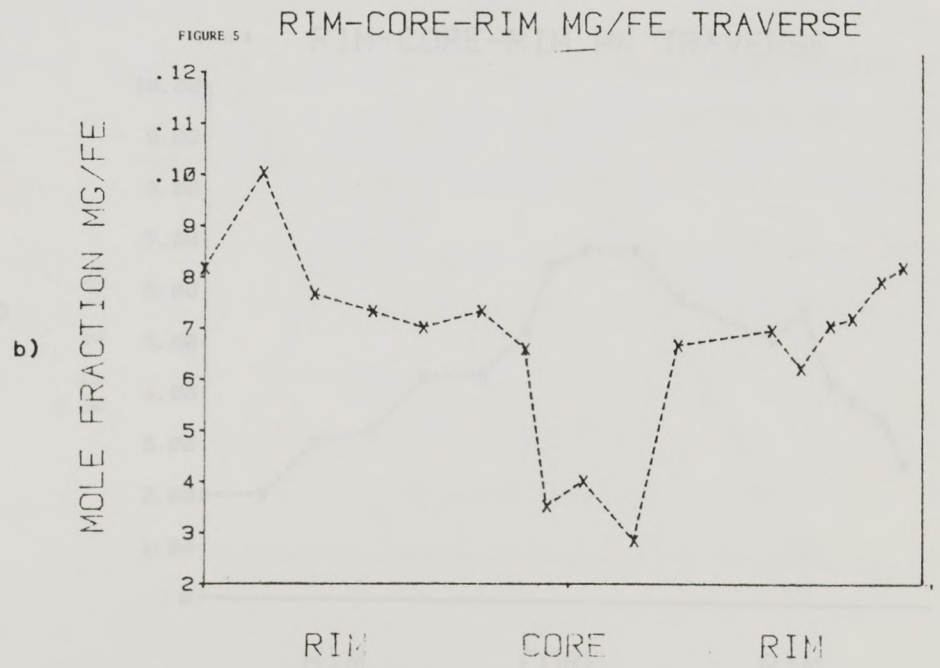


Fig.32a-d. Rim-core-rim traverses across a garnet in sample DI-5. Note the consistent zonation characteristics between the four traverses.

c)

FIGURE 7 RIM-CORE-RIM MG TRAVERSE


d)

FIGURE 8 RIM-CORE-RIM MN TRAVERSE

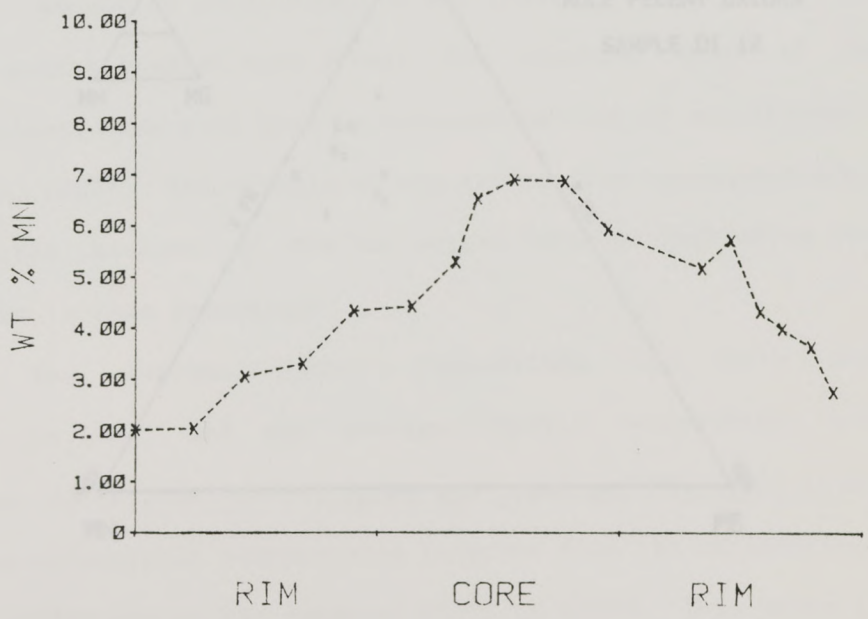

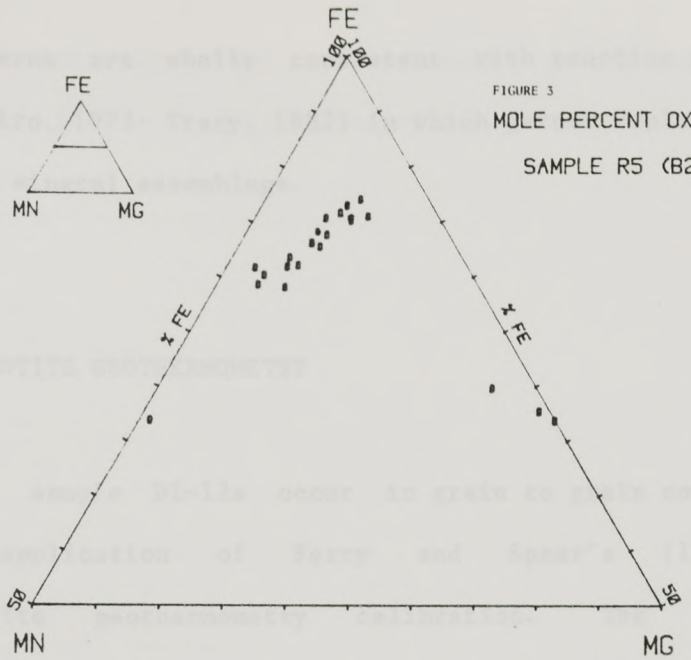


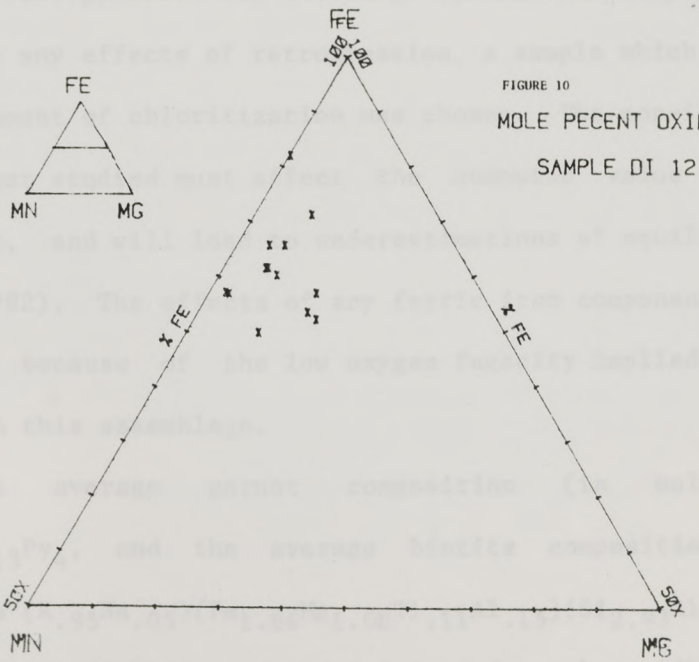


Fig.33. Ternary plots of data accumulated for garnets in samples DI-5 (a) and DI-12a (b).

These patterns are wholly consistent with reaction partitioning models (eg. Miyashiro, 1973· Tracy, 1982) in which garnet replaces chlorite in the metamorphic mineral assemblage.

## GARNET - BIOTITE GEOTHERMOMETRY

Garnets in sample DI-12a occur in grain to grain contact with biotite, allowing application of Ferry and Spear's (1978) experimental garnet-biotite geothermometry calibration. The value of such a determination in the present case depends upon the magnitude of the effects of partial retrogression and the large spessartine component in the garnet. To minimize any effects of retrogression, a sample which had undergone a minimal amount of chloritization was chosen. The non-ideal behavior of Mn in the garnet studied must affect the computed value of the partition coefficient, and will lead to underestimations of equilibrium temperatures (Essene, 1982). The effects of any ferric iron components are judged to be negligible because of the low oxygen fugacity implied by the presence of graphite in this assemblage.

The average garnet composition (in mole fractions) is $Al_{67}Gr_{16}Sp_{13}Py_4$, and the average biotite composition, normalized to 8 cations, is $(K_{.95}Na_{.05})(Fe_{1.66}Mg_{1.08}Ti_{.11}Al_{.15})(Si_{2.93}Al_{1.72})O_{10}OH_2$. Thus, maximum metamorphic temperatures inferred from the calibration of Ferry and Spear (1978) are in the range of 460°C to 485°C. This value lies within a geologically reasonable temperature range in light of the low $fo_2$ values,

and is consistent with other geothermometry measurements in the basin (Thomas, 1981; Burks, unpublished work).

BIBLIOGRAPHY

Arthaud, F., and Matte, P. 1977. Late Paleozoic strike-slip faulting in southern Europe and northern Africa: Results of a right-lateral shear zone between Appalachians and the Urals. GSA Bull. 88, 1305-1320.

Beach, A. and Jack, S. 1981. Syntectonic vein development in a thrust sheet from the external French Alps. Tectonophysics 81, 67-84.

Bell, T.H. 1981. Foliation development: the contribution, geometry, and significance of progressive, bulk, inhomogeneous shortening. Tectonophysics 75, 273-296.

Berryhill, A.W. and Mosher, S. 1983. Fault-related polyphase deformation on Dutch Island, Rhode Island. G.S.A. Abstracts with Programs 15, 129.

Berryhill, A.W. In press. Structural analysis of progressive deformation within a complex strike-slip fault system. G.S.A. Abstracts with Programs 16.

Biot, M.A. 1965. Theory of similar folding of the first and second kind. G.S.A. Bull. 76, 251-258.

Burks, R. J. 1981. Alleghenian deformation and metamorphism in Narragansett Basin, Rhode Island. M.A. thesis, Univ. of Texas at Austin, 91p.

Burks, R.J., Mosher, S. and Murray, D.P. 1981. Alleghenian deformation and metamorphism of southern Narragansett Basin. In: Guidebook of Geologic Field Studies in Rhode Island and Adjacent Areas (edited by Boothroyd, J.C. and Hermes, O.D.) Univ. of Rhode Island, Kingston, Rhode Island, 184-265.

Coward, M.P. 1976. Strain within ductile shear zones, Tectonophysics 34, 181-197.

Deere, W.A., Howie, L.A. and Zussman, J. 1966. An Introduction to the Rock-forming Minerals, Longman Group, Ltd., London, 528 p.

Essene, E.J. 1982. Geologic thermometry and barometry. In: Reviews in Mineralogy (edited by Ferry, J.M.) 10, Min. Soc. of Am., 153-206.

Farrens, C. M. 1982. Styles of deformation in the southeastern Narragansett Basin, Rhode Island and Massechussetts. M.A. thesis, Univ. of Texas at Austin, Austin, Texas, 66p.

Ghosh, S.K. and Ramberg, H. 1976. Reorientation of inclusions by combination of pure shear and simple shear. Tectonophysics 34, 1-70.

Grew, E.S., and Day, H.W. 1972. Staurolite, kyanite, and andalusite from the Narragansett Basin of Rhode Island. U.S.G.S. Prof. Paper 800-D, 151-167.

Hanmer, S. 1981. Tectonic significance of the northestern Gander Zone, Newfoundland: an Acadian ductile shear zone. Can. J. Earth Sci. 18, 120-135.

Harding, T.P. 1973. The Newport-Englewood trend, California - an example of wrenching style of deformation. A.A.P.G. Bull. 57.

Helmstaedt, H. and Dixon, J.M. 1980. Superposed crenulation cleavages resulting from progressive deformation. In: Analytical studies in structural geology (edited by Schwerdtner, W.M. et. al.) Tectonophysics 66, 115-126.

Henderson, M.C. 1983. Narragansett Basin, Rhode Island: role of preexisting intrabasinal horsts and grabens in Alleghanian deformation. G.S.A. Abstracts with Programs 15, 129.

Henderson, M.C. In prep. Narragansett Basin, Rhode Island: role of preexisting intrabasinal horsts and grabens in Alleghenian deformation. M.A. thesis, Univ. of Texas at Austin, Austin, Texas.

Kent, D.V. 1982. Paleomagnetic evidence for post-Devonian displacement of the Avalon Platform (Newfoundland). J. Geophys. Res. 87, 8709-8716.

Kent, D.V., and Opdyke, N.D. 1978. Paleomagnetism of the Devonian Catskill red beds: Evidence for motion of the coastal New England-Canadian Maritime region relative to cratonic North America. J. Geophys. Res. 83, 4441-4450.

Lyons, J.B., Boudette, E.L. and Aleinikoff, J.N. 1982. The Avalonian and Gander zones in central eastern New England. Spec. Pap. Geol. Assoc. Can. 24, 43-66.

McMaster, R.L., de Boer, J. and Collins, B.P. 1980. Tectonic development of southern Narragansett Bay and offshore Rhode Island, Geology 8, 496-500.

Miyashiro, A. 1973. Metamorphism and Metamorphic Belts. The Gresham Press, Old Working, Surrey, 491 p.

Mosher, S. 1976. Pressure solution as a deformation mechanism in Pennsylvanian conglomerates from Rhode Island. J. Geol. 84, 355-364.

Mosher, S. 1978. Pressure solution as a deformation mechanism in the Purgatory Conglomerate. Ph. D. thesis, Univ. of Ill. at Urbana, Urbana, 181 p.

Mosher, S. 1980. Pressure solution deformation of conglomerates in shear zones, Narragansett Basin, Rhode Island. J. Struct. Geol. 2, 219-226.

Mosher, S., and Wood, D.S. 1976. Mechanics of Alleghenian deformation in the Pennsylvanian of Rhode Island. In: Geology of Southeastern New England (edited by Cameron, B.) New England Intercollegiate Geological Conference, 68th Annual Meeting, 472-490.

Mosher, S. 1983a. Late Paleozoic deformation of the Narragansett Basin, Rhode Island and Massachusetts.

Mosher, S. 1983b. Kinematic history of the Narrgansett Basin, Massachusetts and Rhode Island: Constraints on late Paleozoic plate reconstructions. Tectonics 2, 327-344.

Murray, D.P., and Raben, J. 1980. The metamorphism of carbonaceous material, Narragansett Basin, southeastern New England, U.S.A. Int. Geol. Congr. Abstr. - Congr. Geol. Int., Resumes 26, 1064.

Mutch, T.A. 1968. Pennsylvanian non-marine sediments of the Narragansett Basin of Massachusetts and Rhode Island. In: Late Paleozoic and Mesozoic Continental Sedimentation, Northeastern North America (edited by deVries Klein, G.) G.S.A. Special Paper 106, 177-209.

Nicolas, A., and Poirier, J.P. 1976. Crystalline plasticity and solid state flow in metamorphic rocks. John Wiley and Sons, New York.

Ramberg, H. 1964. Selective buckling of composite layers with contrasted rheological properties, a theory for simultaneous formation of several orders of folds. Tectonophysics 1, 307-341.

Ramsay, D.M. 1979. Analysis of rotation of folds during progressive deformation. G.S.A. Bull. 90, 732-738.

Ramsay, J.G. 1980. Shear zone geometry: a review. J. Struct. Geol. 2, 83-99.

Ramsay, J.G. and Graham, R.H. 1970. Strain variation in shear belts. Can. Jour. Earth Sci. 7, 786-813.

Rhodes, S. and Gayer, R.A. 1977. Non-cylindrical folds, linear structures in the X direction and mylonite development during translation of the Caledonian Kalak nappe complex of Finmark. Geol. Mag. 114, 329-341.

Sanderson, D.J. 1973. The development of fold axes oblique to the regional trend. Tectonophysics 16, 55-70.

Sanderson, D.J. 1979. The transition from upright to recumbant folding in the Variscan fold belt of southwest England: a model based on the kinematics of simple shear. J. Struct. Geol. 1, 171-186.

Shaler, N.S., Woodsworth, J.B. and Foerste, A.F. 1899. Geology of the Narragansett Basin. U.S.G.S. Monogr. 33, 402 pp.

Skehan, S.J., and Murray, D.P. 1979. Geology of the Narragansett Basin, southeastern Massachusetts and Rhode Island. In: Carboniferous Basins of Southeastern New England (edited by Cameron, B.) American Geological Institute, Falls Church, Virginia, 7-35.

Skjernaa, L. 1980. Rotation and deformation of randomly oriented planar and linear structures in progressive simple shear. J. Struct. Geol. 2, 101-109.

Thomas, K.J. 1981. Deformation and metamorphism in the central Narragansett Basin of Rhode Island. M.A. thesis, Univ. of Texas at Austin, Austin, Texas, 96 p.

Tracy, R.J. 1982. Compositional zoning and inclusions in metamorphic minerals. In: Reviews in Mineralogy (edited by Ferry, J.M.) 10, Min. Soc. of Am., 355-397.

Trcionski, W.E. 1977. Canadian Mineral. 15, 250,256.

Wilcox, R.E., Harding, T.P. and Seely, D.R. 1974. Basin wrench tectonics. A.A.P.G. Bull 57, 74-94.

Williams, G.D. 1978. Rotation of contemporaneous folds into the X-direction during overthrust processes in Laksefjord, Finmark. Tectonophysics 48, 29-40.

Winsor, C.N. 1981. Syntectonic vein and fibre growth associated with multiple slaty cleavage development in the Lake Moondarra area, Mount Ida, Australia. Tectonophysics 92, 195-210.

The vita has been removed from the digitized version of this document.